Circadian, Carbon, and Light Control of Expansion Growth and Leaf Movement[1][OPEN]

Federico Apelt,[a] David Breuer,[a] Justyna Jadwiga Olas,[b] Maria Grazia Annunziata,[a] Anna Flis,[a,2] Zoran Nikoloski,[a] Friedrich Kragler,[a] and Mark Stitt[a,3]

[a]Max Planck Institute of Molecular Plant Physiology, 14476 Potsdam, Germany
[b]University of Potsdam, 14476 Potsdam, Germany

ORCID IDs: 0000-0003-3450-9369 (F.A.); 0000-0002-3211-5940 (D.B.); 0000-0001-8593-1741 (J.J.O.); 0000-0002-4311-6738 (M.G.A.); 0000-0003-2671-6763 (Z.N.); 0000-0001-5308-2976 (F.K.); 0000-0002-4900-1763 (M.S.).

We used Phytotyping[4D] to investigate the contribution of clock and light signaling to the diurnal regulation of rosette expansion growth and leaf movement in Arabidopsis (*Arabidopsis thaliana*). Wild-type plants and clock mutants with a short (*lhycca1*) and long (*prr7prr9*) period were analyzed in a T24 cycle and in T-cycles that were closer to the mutants' period. Wild types also were analyzed in various photoperiods and after transfer to free-running light or darkness. Rosette expansion and leaf movement exhibited a circadian oscillation, with superimposed transients after dawn and dusk. Diurnal responses were modified in clock mutants. *lhycca1* exhibited an inhibition of growth at the end of night and growth rose earlier after dawn, whereas *prr7prr9* showed decreased growth for the first part of the light period. Some features were partly rescued by a matching T-cycle, like the inhibition in *lhycca1* at the end of the night, indicating that it is due to premature exhaustion of starch. Other features were not rescued, revealing that the clock also regulates expansion growth more directly. Expansion growth was faster at night than in the daytime, whereas published work has shown that the synthesis of cellular components is faster in the day than at nighttime. This temporal uncoupling became larger in short photoperiods and may reflect the differing dependence of expansion and biosynthesis on energy, carbon, and water. While it has been proposed that leaf expansion and movement are causally linked, we did not observe a consistent temporal relationship between expansion and leaf movement.

Leaf expansion growth changes in a time-of-day-dependent manner in Arabidopsis (*Arabidopsis thaliana*; Wiese et al., 2007; Poiré et al., 2010; Yazdanbakhsh et al., 2011; Ruts et al., 2012; Dornbusch et al., 2014; Apelt et al., 2015). This is partly due to changes in carbohydrate allocation: while growth can use photosynthetically fixed C in the light, growth in the night depends on reserves like starch that accumulate in the light and are remobilized at night (Smith and Stitt, 2007; Graf et al., 2010). Growth dynamics are partly due to changes in water status linked to increased evapotranspiration in the light (Pantin et al., 2011, 2012, 2013). In addition, a role for the circadian clock is revealed by observations that growth oscillations are maintained in continuous light (LL; Wiese et al., 2007; Poiré et al., 2010; Dornbusch et al., 2014).

The plant clock can be viewed as an interconnected repressilator with coupled dawn, day, dusk, and evening loops (Nakamichi, 2011; Pokhilko et al., 2012; Carré and Veflingstad, 2013; Fogelmark and Troein, 2014; Supplemental Fig. S1). The dawn genes *LATE ELONGATED HYPOCOTYL* (*LHY*) and *CIRCADIAN CLOCK ASSOCIATED1* (*CCA1*) peak at around dawn, followed by the day genes (*PSEUDO RESPONSE REGULATOR7* [*PRR7*] and *PPR9*), the dusk genes (*PRR5*, *TIME OF CAB EXPRESSION1* [*TOC1*], and *GIGANTEA*), and evening complex (EC) components (*EARLY FLOWERING3* [*ELF3*], *ELF4*, and *LUX ARRHYTHMO*). In some cases, the molecular interactions between clock components are still a matter of debate; for example, whereas earlier models proposed a positive interaction between the dawn and day genes, recent studies indicate that *CCA1* and *LHY* directly repress the expression of *PRR7* and *PRR9* (Adams et al., 2015; Kamioka et al., 2016). Sequential expression of these core clock components orchestrates successive waves of the expression of output genes, affecting up to

[1] This work was supported by the Max Planck Society, the European Union (collaborative project TiMet under contract no. 245143), and an International Max Planck Research School stipend (to D.B.).

[2] Current address: Australian Research Council Centre of Excellence for Translational Photosynthesis, Plant Science Division, Research School of Biology, Australian National University, Acton, Australian Capital Territory 2601, Australia.

[3] Address correspondence to mstitt@mpimp-golm.mpg.de.

The author responsible for distribution of materials integral to the findings presented in this article in accordance with the policy described in the Instructions for Authors (www.plantphysiol.org) is: Mark Stitt (mstitt@mpimp-golm.mpg.de).

F.A. grew and imaged plants, implemented the analysis pipeline, analyzed data, wrote the first draft of the article, and aided in all further edits; D.B. implemented the analysis pipeline and analyzed data; J.J.O., M.G.A., and A.F. contributed to the data collection; Z.N. supervised D.B. and suggested analysis improvements; M.S. and F.A. supported by D.B. and F.K wrote the article; F.K. suggested experiments; M.S. conceived the study, suggested experiments, and, with F.K., supervised the project.

[OPEN] Articles can be viewed without a subscription.
www.plantphysiol.org/cgi/doi/10.1104/pp.17.00503

half the transcriptome (Harmer et al., 2000; Michael et al., 2008). The clock has a period of about 24 h, but this is shortened to about 17 h in the *lhycca1* double mutant (Alabadí et al., 2002; Mizoguchi et al., 2002; Salomé and McClung, 2005) and extended to 28 to 32 h in the *prr7prr9* double mutant (Farré et al., 2005; Salomé and McClung, 2005; Flis et al., 2015).

The circadian regulation of expansion growth has been studied intensively in germinating seedlings. Hypocotyl elongation typically occurs close to dawn in a light-dark cycle and close to subjective dusk in LL (Dowson-Day and Millar, 1999; Nozue et al., 2007). The clock acts via EC, whose activity peaks at dusk and represses the growth-promoting transcription factors *PHYTOCHROME INTERACTING FACTOR4* (*PIF4*) and *PIF5* (Nusinow et al., 2011). The *elf3* mutant has a strongly elongated hypocotyl (Dowson-Day and Millar, 1999; Niwa et al., 2009; Nusinow et al., 2011), *PIF4* overexpression also leads to long hypocotyls (Sun et al., 2012), and *pif4pif5* has shorter hypocotyls than wild-type plants (Lorrain et al., 2008). ELF3 also directly interacts with PIF4 to regulate hypocotyl elongation in an EC-independent manner (Nieto et al., 2015).

Less is known about the circadian regulation of expansion growth in vegetatively growing plants. Ruts et al. (2012) showed that *CCA1*-expressing lines and the arrhythmic *prr5prr7prr9* mutant exhibit decreased leaf expansion growth at night relative to the light period. Dornbusch et al. (2014) reported that leaf elongation peaked at ZT2 to ZT4 (Zeitgeber time scale) in wild-type plants and that this peak was shifted forward to close to dawn in *elf3* mutants, whereas *PIF4* overexpressors and *pif4pif5* double mutants resembled wild-type plants except for a smaller amplitude of the oscillation in *pif4pif5* (Dornbusch et al., 2014). Root elongation peaks at about ZT2 in wild-type Arabidopsis, and a growth oscillation is maintained in LL, whereas in *elf3* root, elongation peaks at about ZT12 in a light-dark cycle and occurs throughout the 24-h cycle in LL (Yazdanbakhsh et al., 2011). These findings point to different mechanisms underlying circadian rhythms of expansion in young hypocotyls, seedling roots, and rosette leaves.

In vegetatively growing plants, the clock also may exert an indirect effect on growth via its role in the regulation of starch turnover. The C supply limits the growth of Arabidopsis in short or neutral (i.e. having a similar length of day and night) photoperiods (Gibon et al., 2009; Hädrich et al., 2012; Sulpice et al., 2014). The clock paces the rate of starch breakdown such that starch is almost exhausted at the next anticipated dawn (i.e. ~24 h after the previous dawn in wild-type plants; Lu et al., 2005; Smith and Stitt, 2007; Graf et al., 2010; Graf and Smith, 2011; Pyl et al., 2012; Stitt and Zeeman, 2012; Scialdone et al., 2013). Starch is prematurely exhausted in the short-period *lhycca1* double mutant and when wild-type plants are grown in a 14-h-light/14-h-dark regime (T28 cycle), whereas large amounts of starch remain at dawn when wild-type plants are grown in an 8.5-h-light/8.5-h-dark cycle (T17 cycle; Graf et al., 2010; Graf and Smith, 2011; Scialdone et al., 2013). Studies in the starchless *pgm* mutant (which lacks plastidial phosphoglucomutase) have shown that the exhaustion of C reserves activates protein catabolism and inhibits protein and cell wall synthesis and leaf expansion (Gibon et al., 2004; Usadel et al., 2008; Izumi et al., 2013; Apelt et al., 2015; Ishihara et al., 2015). The importance of the circadian regulation of starch turnover is illustrated by the observation that root elongation is inhibited in the last hours of the night in *lhycca1*, following the premature exhaustion of starch, and this inhibition is reversed by adding Suc to the growth medium (Yazdanbakhsh et al., 2011). Yanovsky and Kay (2002) and Dodd et al. (2005) proposed that growth deficits in mutants with an altered clock period can be reversed by matching the duration of the external light-dark cycle to the internal clock period, and Graf et al. (2010) proposed that this can be partly explained because starch degradation is paced to dawn, as anticipated by the clock in a given genotype. Nevertheless, *toc1* and *ztl* mutants grew better under T24 than either T20 or T28, independently of their endogenous period (Graf et al., 2010), indicating that these mutants are impaired in growth for other reasons than a mismatch between clock period and the external light-dark cycle.

Plants also show rhythmic changes in leaf angle, termed hyponasty (Whippo and Hangarter, 2009; Dornbusch et al., 2012, 2014). Hyponastic movement is regulated by the clock (Farré, 2012). In species that show rapid reversible leaf movement, like members of the Leguminosae, movement is mediated by turgor changes in specialized cells at the base of the petiole, termed the pulvini (Whippo and Hangarter, 2009). In species that lack pulvini, like Arabidopsis, movement is thought to be due to differential enlargement of cells in the adaxial and abaxial regions of the petiole (Polko et al., 2012; Rauf et al., 2013). Little is known about the causal relationship between leaf expansion and leaf movement. Dornbusch et al. (2014) noted a time delay of ~3 h between leaf elongation and leaf movement. It is uncertain if this delay reflects a sequential chain of events or is due to them being regulated at different times by a third factor like the clock.

In the past, analysis of leaf expansion and leaf movement was hampered by a lack of imaging methods to deconvolute their overlapping effects (Spalding and Miller, 2013). In a two-dimensional (2D) image, it is difficult to distinguish whether a change in apparent object size is due to an actual change in size of the object, movement of the object toward or away from the camera, or a change in the angle subtended by the object. Typical growth rates of Arabidopsis are 0.2 to 0.3 mg fresh weight mg^{-1} fresh weight d^{-1} (Sulpice et al., 2014), which is of the order of 1% per hour, whereas Arabidopsis leaf angle can change by several degrees per hour (Dornbusch et al., 2014; Apelt et al., 2015). Two complementary technologies were recently developed to deconvolute leaf elongation or leaf expansion from leaf movement. One combines 2D camera images with laser scanning to reconstruct a three-dimensional (3D) image of an Arabidopsis rosette (Dornbusch et al., 2012). The other, called Phytotyping^{4D},

uses a light-field (plenoptic) camera that delivers a 2D focus image and a distance image, which are combined to reconstruct a 3D surface image (Apelt et al., 2015). Phytotyping^{4D} was used previously to compare diurnal changes in leaf expansion and leaf movement in wild-type Columbia-0 (Col-0) and the starchless *pgm* mutant (Apelt et al., 2015). We now use Phytotyping^{4D} to investigate the role of the clock in regulating rosette expansion and hyponasty in Arabidopsis.

RESULTS

Experimental Setup and Imaging System

Rosette relative expansion rate (RER; the increase in area per unit of area per hour [$mm^2\ mm^{-2}\ h^{-1}$]) and leaf movement were monitored using a light-field camera-based imaging system (Apelt et al., 2015; Supplemental Fig. S2; Supplemental Methods S1). The experiments are listed in Supplemental Table S1. The first experiment compared *lhycca1*, *prr7prr9*, and the corresponding wild types (Wassilewskija-2 [Ws-2] and Col-0) in a 12-h-light/12-h-dark T24 cycle. *lhycca1* is defective in dawn clock components and has a short period, whereas *prr7prr9* is defective in day components and has a long period (see introduction and Supplemental Fig. S1). The second experiment investigated *lhycca1* and Ws-2 in a T17 cycle (8.5 h of light/8.5 h of dark) and *prr7prr9* and Col-0 in a T28 cycle (14 h of light/14 h of dark). Phenotypes of clock mutants with an altered period can be due to a mismatch between the internal clock period and the external light-dark cycle and/or to loss of clock outputs (Yanovsky and Kay, 2002; Dodd et al., 2005; Graf et al., 2010). This experiment was designed to reveal which features of the phenotype are recovered by matching the external light-dark cycle to the internal clock period and are probably due to the change in clock period and which are not recovered in a matching T-cycle and are probably due to loss of outputs that require the mutated clock components. In addition, this experiment should reveal what happens when wild-type plants are grown in a non-matching external cycle. The third experiment investigated *elf3*, *pif4pif5*, and the corresponding wild types (Ws-2 and Columbia-4 [Col-4]). These mutants are deficient in genes that regulate the timing of hypocotyl elongation (Nusinow et al., 2011). They were analyzed for diurnal changes of leaf elongation and hyponasty in vegetatively growing plants under strong far-red light by Dornbusch et al. (2014). The above experiments were all performed in a neutral photoperiod. To distinguish between endogenous rhythms and acute responses to light, we also analyzed RER and leaf movement in wild-type plants growing in an 8-h/16-h (short day [SD]) or a 16-h/8-h (long day [LD]) light-dark cycle and after transfer to LL or continuous darkness (DD).

Experiments were typically performed on 10 to 20 plants for seven light-dark cycles, usually starting 17 d after sowing (DAS), with images being captured every 12 min for each plant (Supplemental Table S1). To calculate time-resolved estimates of RER and leaf angles, data for each plant were averaged across all the light-dark cycles, means and SD across replicates were computed, and the resulting time series were smoothed using a 1-h sliding median. Examples of photographic images are provided in Supplemental Figure S3, and average values for the increase in total rosette area with time are provided in Supplemental Figure S4. Analysis of data for wild-type Col-0 and Ws-2 growing in a neutral T24 photoperiod revealed that variations in RER and leaf angle were equally partitioned between replicate plants and the day of measurement (Supplemental Fig. S5A). Heat maps showing the time series for individual plants averaged across 7 d for *prr7prr9*, *lhycca1*, and the wild types Col-0 and Ws-2 are provided in Supplemental Figure S5B. Time series for each individual plant are provided for all genotypes and treatments in Supplemental Figure S6. Agreement between individual plants was very good for leaf angle and reasonable for RER, although there was sometimes more noise (especially for Ws-2 and *lhyccca1* in T17 and *elf3* in T24). As experimental noise was higher in the RER measurements, we carried out independent Student's *t* tests, which were applied to each time point individually as well as to 1-h sliding windows and two-way ANOVA with genotype and plant as factors. All tests were applied before averaging and smoothing the time series (Supplemental Fig. S7). We found that significant differences between time series were mainly due to genotype, while plant and interaction between genotype and plant had negligible contributions. As discussed by Apelt et al. (2015), one major source of noise is high leaf angle, with noise increasing as leaf angle rises above 25° for much of the rosette area. The proportion of the rosette surface at different leaf angles is illustrated for exemplary treatments in Supplemental Figure S8. An additional source of noise in *elf3* was the long hypocotyl, which led to plants sometimes changing their tilt and introducing noise into the data series, including areas of the rosette with a negative angle.

Diurnal Changes in RER in Wild Types and Clock Mutants in a Neutral T24 Cycle

We first present results for RER (Figs. 1 and 2; Supplemental Fig. S9). The plots include *P* values obtained using independent Student's *t* tests (denoted p_t), comparing data within a sliding window of 1 h, and significant *P* values ($P < 0.05$) from Student's *t* tests for single time points shown as dots above the bottom panel; for additional analyses including two-way ANOVA, see Supplemental Figure S7.

The diurnal changes of RER in Col-0 in a 12-h photoperiod (Fig. 1A) resemble those reported by Apelt et al. (2015). After dawn, there was a rapid decline to a minimum at about ZT1, a recovery to a peak at about ZT4, a slow decline during the remainder of the light period, a large transient increase and decrease after dusk, and a gradual increase until ZT18 to a rate similar to or slightly higher than in the last part of the light

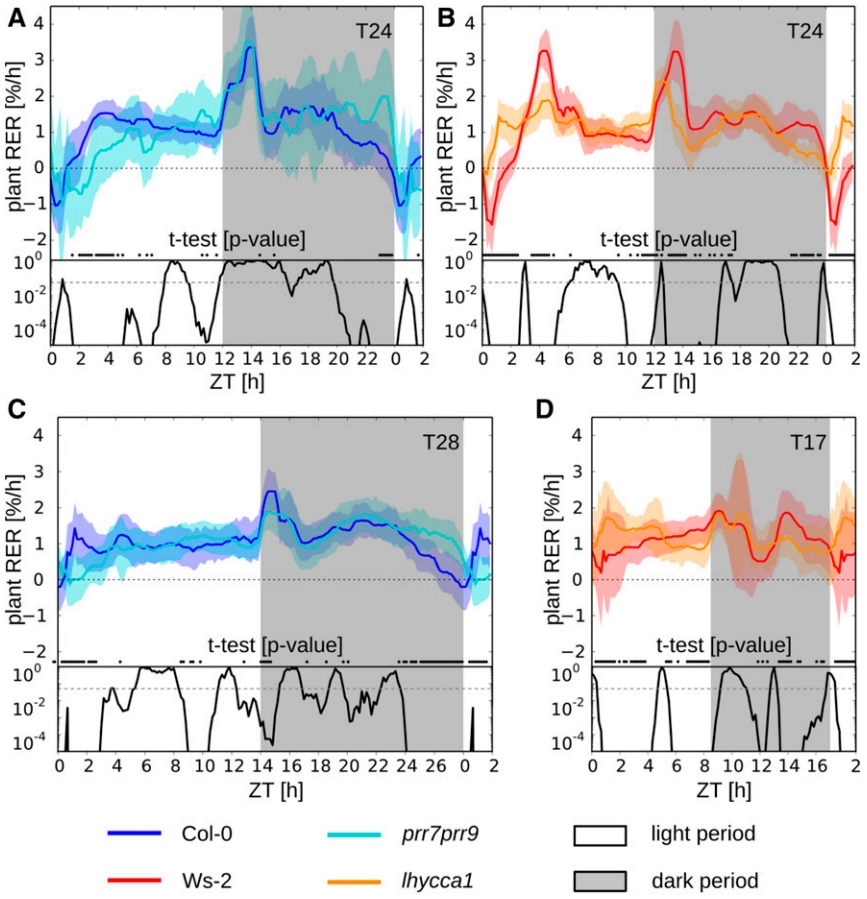

Figure 1. Diurnal RERs of wild-type Col-0 and Ws-2 and the *lhycca1* and *prr7prr9* clock mutants in T24, T17, and T28 cycles in neutral-day conditions. Photosynthetically active radiation was 160 μmol m^{-2} s^{-1}, with 20°C in the light and 18°C in the dark. A and B, Diurnal RER of Col-0, Ws-2, *lhycca1*, and *prr7prr9* in a 12-h-light/12-h-dark cycle (T24). C, Diurnal RER of Col-0 and *prr7prr9* in a 14-h-light/14-h-dark cycle (T28). D, Diurnal RER of Ws-2 and *lhycca1* in an 8.5-h-light/8.5-h-dark cycle (T17). Diurnal RER was averaged for each plant over all sequential T-cycles, and means and SD were computed for $n \geq 10$ plants for each genotype, represented by lines and color-shaded areas, respectively, and a sliding median filter with a window of 1 h was applied (Supplemental Table S1; Supplemental Figs. S4–S7). Time is given in hours after dawn (ZT). Points above the bottom panels denote significant *P* values ($P < 0.05$) from individual Student's *t* tests for differences in mean RER for nonsmoothed data (Supplemental Fig. S7), and bottom panels indicate *P* values from Student's *t* tests applied over a 1-h sliding window, where $P < 0.05$ (dashed gray line) was considered significant.

period. This rate was maintained until the end of the night. The decrease immediately before dawn may be partly an artifact of time averaging, as the very low or even negative RER after dawn will depress the estimated rate immediately before dawn. Diurnal changes in Ws-2 (Fig. 1B) and Col-4 (Supplemental Fig. S9A) resembled that in Col-0, except that the peak at ZT4 was more marked in Ws-2.

Compared with the reference wild type Col-0, *prr7prr9* showed increased RER toward the end of the night (ZT20–ZT24) and low RER in the first half of the light period (ZT0–ZT8; Fig. 1A). Compared with the reference wild type Ws-2, *lhycca1* (Fig. 1B) showed higher RER after dawn (ZT0–ZT2), an attenuated peak at ZT4, similar RER for most of the remaining light period, higher RER just before dusk (ZT11), an attenuated stimulation of RER after dusk (ZT13 and ZT14), lower RER between ZT14 and ZT16, and a decrease of RER to low values between ZT21 and ZT24. The changes in *prr7prr9* and *lhycca1* could be seen in almost all individual plants (Supplemental Figs. S5 and S6). They were highly significant after Student's *t* testing with a 1-h sliding window ($p_t < 0.00001$; Fig. 1, A and B) and were also significant in Student's *t* tests and two-way ANOVAs on individual time points ($P < 0.05$; Fig. 1, A and B; Supplemental Figs. S7 and S9, A and B). Diurnal changes in *pif4pif5* resembled those in Col-4 (Supplemental Figs. S7E and S9A), with the only sustained significant difference ($p_t < 0.01$) being a smaller peak at ZT4. *elf3* mutants have an extreme growth phenotype with elongated hypocotyls and high leaf angle (Zagotta et al., 1996; Dowson-Day and Millar, 1999; Dornbusch et al., 2014; Supplemental Fig. S3). This led to fluctuations in image acquisition, and the estimates of RER are extreme approximations (Supplemental Figs. S6, S7F, and S9B).

Diurnal Changes in RER in *lhycca1* and *prr7prr9* in Non-T24 Light-Dark Cycles

A matching T28 cycle rescued some features of the diurnal growth phenotype of *prr7prr9* (compare Fig. 1, C and A). RER declined in *prr7prr9* in the last part of the night in a T28 cycle, whereas it remained high until the end of the night in a T24 cycle. This decline was significant when the time series for *prr7prr9* in T24 and T28 were aligned on dawn (Supplemental Fig. S10A). Nonetheless, RER at the end of the night was still higher in *prr7prr9* in T28 than in Col-0 in T24 (Supplemental Fig. S10B). However, other features were not rescued, including the low RER in the first 3 to 4 h of the light period, which was observed in both T28 and T24 cycles. A matching T17 cycle rescued some but not all features for *lhycca1* (compare Fig. 1, D and B). Whereas RER was

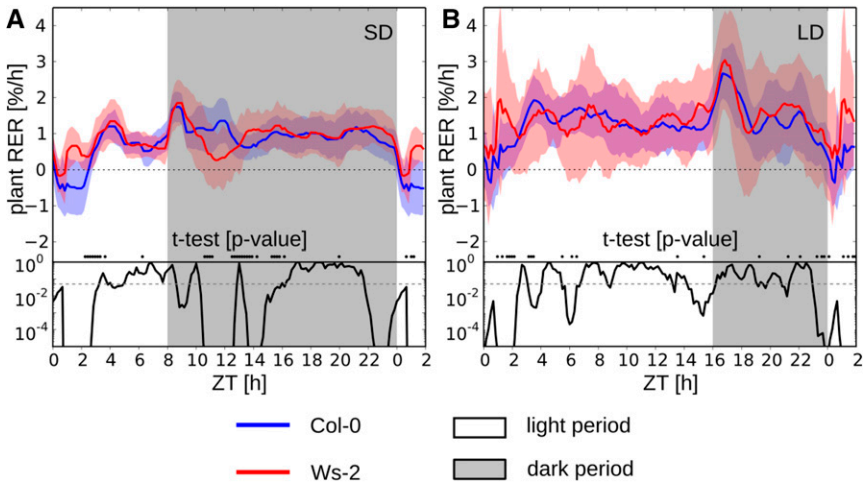

Figure 2. Diurnal RERs of wild-type Col-0 and Ws-2 in a T24 cycle in SD and LD photoperiods. Photosynthetically active radiation was 160 μmol m^{-2} s^{-1}, with 20°C in the light and 18°C in the dark. A, Diurnal RER in SD photoperiod with 8 h of light/16 h of dark (T24). B, Diurnal RER in LD photoperiod with 16 h of light/8 h of dark (T24). Diurnal RER was averaged for each plant over all sequential T-cycles, and means and SD were computed for $n \geq 20$ plants for each genotype, represented by lines and color-shaded areas, respectively, and a sliding median filter with a window of 1 h was applied (Supplemental Table S1; Supplemental Figs. S4–S7). Time is given in hours after dawn (ZT). Points above the bottom panels denote significant P values ($P < 0.05$) from individual Student's t tests for differences in mean RER for nonsmoothed data (Supplemental Fig. S7), and bottom panels indicate P values from Student's t tests applied over a 1-h sliding window, where $P < 0.05$ (dashed gray line) was considered significant.

almost zero in the last 4 h of the night in a T24 cycle, growth continued until the end of the night in a T17 cycle (Supplemental Fig. S10, C and D). However, *lhycca1* still showed high RER in the first 1 to 4 h of the light period.

The growth of wild types in non-T24 cycles leads to a mismatch between the external cycle and the internal clock period. When Col-0 was grown in T28, RER declined to low levels earlier in the night than in T24, and RER increased immediately after dawn instead of showing a transient minimum, as in T24 (compare Fig. 1, C and A). Comparison of dawn-aligned time series revealed that the decline in T28 was significant (Supplemental Fig. S10E). When Ws-2 was grown in T17, the transient inhibition of growth after dawn and the peak at ZT4 were attenuated (compare Fig. 1, D and B).

Diurnal Changes of RER in Wild-Type Plants in Short and Long Photoperiods

Col-0 and Ws-2 also showed a transient inhibition of RER after dawn and a transient stimulation of RER after dusk when they were grown in SD and LD (Fig. 2, A and B). Visual inspection of the diurnal RER pattern in short, neutral, and long photoperiods (Figs. 1, A and B, and 2) reveals that the transient peak after dusk shifts back with the timing of dusk, indicating that it is a response to darkening (see below for additional data analyses).

Oscillations of RER after Transfer to LL or DD

To further distinguish between circadian and light responses, Col-0 and Ws-2 were grown for 19 d in a 12-h-light/12-h-dark cycle and shifted to LL for 96 h (Fig. 3, A and B). RER time series were collected for three light-dark cycles before and four cycles after the shift. As the RER estimates for each cycle were calculated separately, there was more noise than in light-dark cycles, where values were averaged across seven cycles. Nevertheless, the main features of the RER diurnal response in Figure 1, A and B, were recapitulated in the light-dark cycles in Figure 3A. After transfer to LL, there was a sustained oscillation of RER, which was stronger in Ws-2 than in Col-0. An averaged RER time series for the last three LL cycles (Fig. 3B) revealed an oscillation of RER with a peak at about ZT4, which was more marked in Ws-2 than in Col-0. Fourier analysis revealed a period of about 24 h in both wild types, which was better defined in Ws-2 than in Col-0 (Fig. 3, C and D). Comparison of measured and randomized data revealed very high z-scores, indicating that the oscillations are significant (Fig. 3, C and D), RER did not decrease after subjective dawn or increase after subjective dusk, providing more evidence that these transients are responses to light. We also grew Col-0 and Ws-2 for 19 d in a 12-h-light/12-h-dark cycle and shifted them to DD (Supplemental Fig. S9, C and D). RER decreased to very low values within 2 to 3 h of extended darkness, as reported previously for root elongation (Yazdanbakhsh et al., 2011).

Comparison of Diurnal Changes in RER across Genotypes and Light Regimes

To allow unbiased comparison, we employed a correlation-based analysis to identify which combinations of T-cycles, photoperiods, and genotypes show

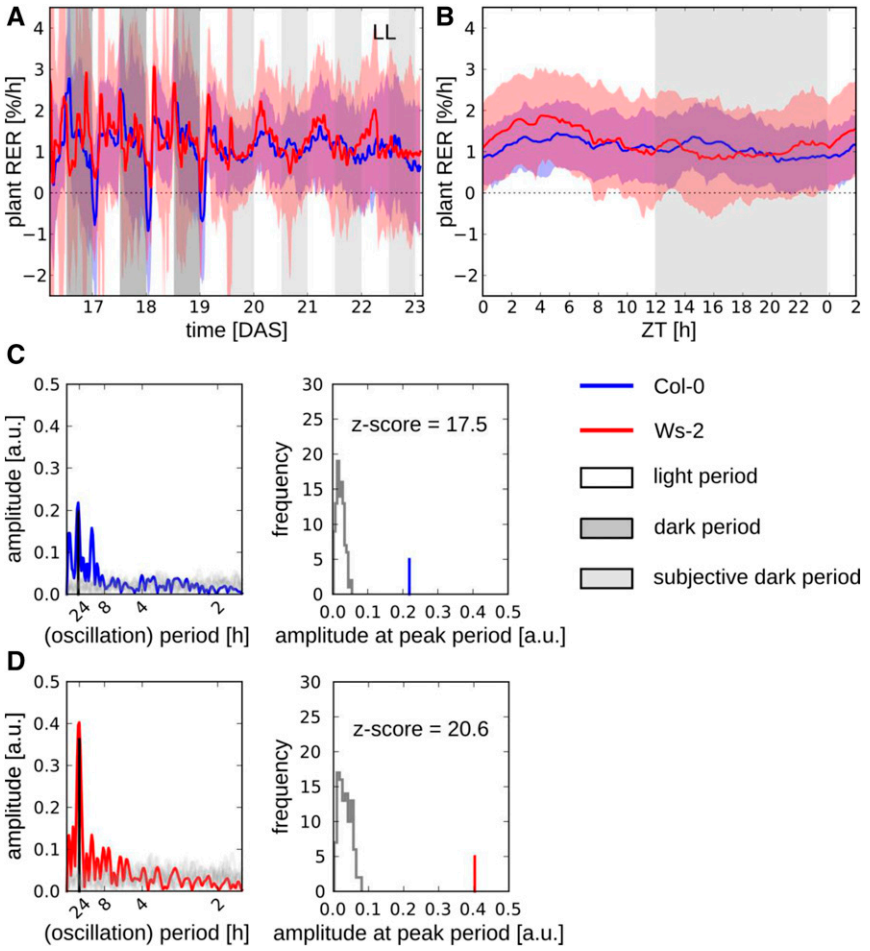

Figure 3. RERs of wild-type Col-0 and Ws-2 before and after the shift from a neutral-day T24 cycle to LL at 19 DAS. Photosynthetically active radiation was 160 μmol m^{-2} s^{-1}, with 20°C in the light and 18°C in the dark. A, Time series of RER before and after transfer of plants to LL. B, Diurnal RER after transfer of plants to LL estimated by averaging the last three cycles in LL. C, Left, Fourier spectrum of the RER in the last three cycles in LL for Col-0 (blue) and Fourier spectra of a set of 100 shuffled RER time series, used as a null model for comparison (pale gray). Right, Quantification of the nonrandomness of periodic oscillation of RER. The blue line and gray histogram indicate peak amplitudes (arbitrary units [a.u.]) of the Fourier spectrum of the biological data and the randomized data, respectively. D, Analogous analysis as in C for Ws-2. The experiment was carried out twice, and the data were combined to calculate the RER time series, with lines representing means and color-shaded areas representing SD ($n \geq 20$ plants for each genotype in each experiment).

similar and which show deviating diurnal RER patterns (Fig. 4). Time-resolved RER values for different genotypes in the same light regime can be plotted directly against each other. The example in Figure 4A shows that there is no correlation between the RER time series data for the short-period mutant *lhycca1* and the long-period mutant *prr7prr9* in a 12-h photoperiod. To correlate treatments with different T-cycle lengths, we aligned them by removing equidistant data points of the longer T-cycle to leave the same number of data points as in the shorter T-cycle (e.g. the T28 cycle was aligned to the T24 cycle by removing every seventh data point from the T28 cycle; Fig. 4B). In comparisons of treatments with different photoperiods, we decided to align the dawns and the dusks, because the large transients after dusk were clearly aligned to dusk rather than the clock cycle. To do this, we differentially removed points in the light and dark periods (e.g. the 16-h photoperiod was aligned to the 12-h photoperiod by removing every fourth data point in the light period from the 16-h photoperiod data set and every third data point in the night from the 12-h photoperiod data set). Squared Pearson correlation coefficients (r^2) were calculated for all pairwise comparisons and used to group the treatments. Therefore, the resulting correlation matrix was clustered using hierarchical single-linkage clustering with a Euclidean distance measure. The number of clusters was chosen based on the silhouette scores, which measure the cluster quality (Rousseeuw, 1987; Supplemental Fig. S11A).

Applying the same clustering procedure to RER in all the neutral photoperiod treatments (Fig. 4C) yielded a cluster containing all the wild types (Col-0, both Ws-2 data series, and Col-4; indicated in orange) in a T24 cycle, a second cluster containing two treatments in which clock period is shorter than the T-cycle (Col-0 in T28 and *lhycca1* in T24; indicated in cyan), and a third cluster containing treatments where clock period is longer than the T-cycle (Ws-2 in T17, *prr7prr9* in T24, and *prr7prr9* in T28; indicated in green). *prr7prr9* in T28 is quite highly correlated (r^2 = 0.63) with *prr7prr9* in a T24 cycle but less strongly with Ws-2 in a T17 cycle (r^2 = 0.31), indicating that its assignment is driven by *prr7prr9* features. *pif4pif5* was intermediate between the wild types in T24 and treatments where the clock period was longer than the T-cycle. *lhycca1* in T17 differed markedly from the other treatments. *elf3* was even less weakly related, but this may be due at least partly to noise. Inclusion of the short-photoperiod and long-photoperiod Col-0 and Ws-2 data did not alter the

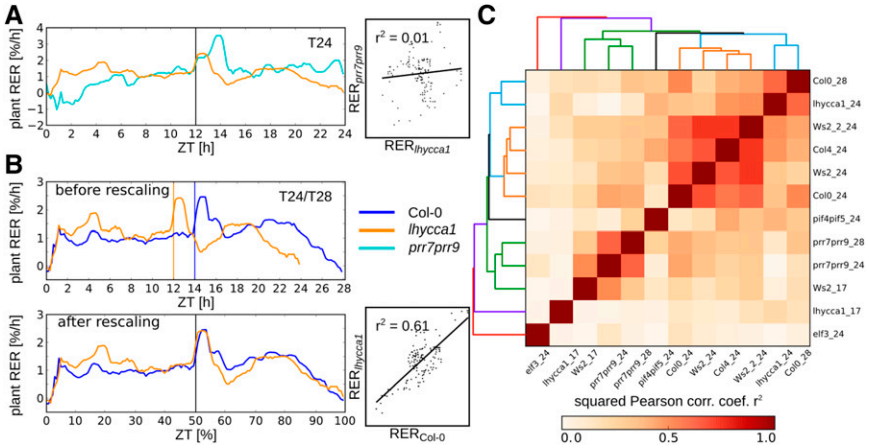

Figure 4. Correlation-based clustering of diurnal RER patterns of wild-type and mutant plants in T24, T17, and T28 cycles in neutral-day conditions. A, Correlation of RER of *lhycca1* and *prr7prr9* in a T24 cycle: RER time series alignment (left) and scatter diagram of *lhycca1* and *prr7prr9* RERs with linear fit indicating their correlation (right). B, Correlation of RER of Col-0 in T28 and *lhycca1* in T24 before rescaling (top) and after rescaling (bottom left), with RER times series alignment and a scatter diagram of rescaled Col-0 and *lhycca1* RERs with linear fit indicating their correlation (bottom right). Rescaling on non-T24 data series was performed by equidistant removal of data points to adjust each time point to the same value relative to the duration of the entire light-dark cycle. C, Clustered heat map of all pairwise squared Pearson correlation coefficients (r^2) between rescaled RER time series of different wild-type and mutant plants. Clustering was performed using hierarchical single-linkage clustering with a Euclidean distance measure. The number of clusters was determined using silhouette scores (Supplemental Fig. S11A), and the resulting clusters are color coded (1, red; 2, blue; 3, green; 4, black; 5, orange; 6, cyan). Time is given in hours after dawn (ZT) or, for rescaled data, as a percentage of the T-cycle length. The original time series data are shown in Figure 1 and Supplemental Figure S9. Ws2_24 and Ws2_2_24 refer to the Ws-2 data series in a 12-h-light/12-h-dark cycle in Figure 1B and Supplemental Figure S9B, respectively. For an analysis that also includes wild-type plants grown in short and long photoperiods, see Supplemental Figure S11B.

basic cluster structure (Supplemental Fig. S11B). Col-0 and Ws-2 in SD clustered with treatments in which clock period is longer than the T-cycle. The LD treatments were separated from the SD treatments: Col-0 in LD grouped close to Col-0 and other wild types in a 12-h-light/12-h-dark cycle, and Ws-2 in LD grouped closer to the treatments where the clock period is shorter than the T-cycle (Col-0 in T28 and *lhycca1* in T24). Although the Arabidopsis clock is predominantly dawn dominant (i.e. entrained to dawn; Seaton et al., 2015; Song et al., 2015), photoperiod does affect clock phase, with a progressive delay in the time at which clock transcripts peak as the photoperiod is lengthened (Flis et al., 2016). This may explain why SD treatments group with the treatments where the clock period is longer than the T-cycle and Ws-2 in LD groups close to treatments where the clock period is shorter than the T-cycle. The differing grouping of the Ws-2 and Col-0 LD treatments might be due to the circadian component being more marked in Ws-2 (Fig. 3).

To aid the inspection of the transients after dawn and dusk, we aligned sections of each time series on dawn and dusk (Fig. 5). There was a transient decrease in RER after dawn, followed by a peak at about ZT4 in almost all genotypes, T-cycles, and photoperiods (Fig. 5A). The transient inhibition was less marked in *lhycca1* in a T24 cycle and, especially, in a T17 cycle. RER increased after dusk in all treatments, peaking at 1.5 to 2 h after dusk in Col-0, Ws-2, and *prr7prr9* in a 12-h-light/12-h-dark cycle and slightly earlier in other treatments (Fig. 5B).

Summarizing, first, the diurnal pattern of RER in wild-type plants includes a circadian component that is more marked in Ws-2 than in Col-0 as well as a transient decrease in RER after the dark-light transition and a transient stimulation of RER after the light-dark transients. Second, the results for wild-type plants and clock mutants support the idea that the diurnal pattern of RER is altered when there is a mismatch between the internal clock period and the external light-dark cycle, with partly opposing responses when the clock period is longer or shorter than the external T-cycle. This is especially clear for the wild-type treatments, whereas *lhycca1* and *prr7prr9* are only partly rescued by matching the T-cycle to the internal clock period. Third, this incomplete rescue indicates that the dawn and day clock components also may exert a more direct impact on RER.

Average RER across the Entire Cycle, the Light Period, and the Dark Period

It has been reported, based on measurements of final biomass, that growth is fastest when the internal clock period matches the duration of the external light-dark cycle (see above). The complex temporal dynamics of RER make it difficult to see, from time-resolved plots, how much growth occurs in a complete light-dark cycle. It is also difficult to see how much growth occurs during the daytime and the night. Therefore, we calculated average RER (expansion growth per hour averaged

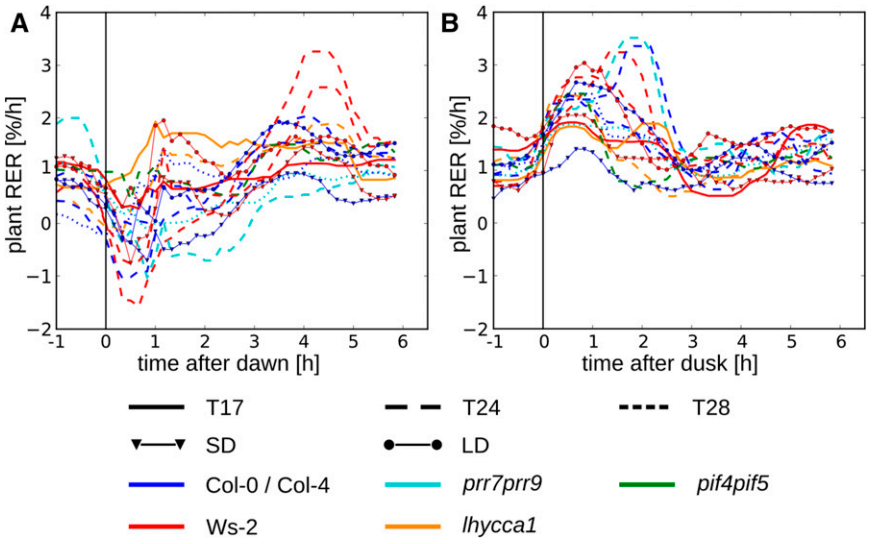

Figure 5. RERs of wild-type and mutant plants at the beginning of the light period and the beginning of the dark period, aligned to dawn and dusk. A, Diurnal RERs aligned to dawn. B, Alignment of RERs to dusk. Time is given in hours after dawn or hours after dusk. The original data are shown in Figures 1 and 2 and Supplemental Figure S9.

over the time interval) across an entire light-dark cycle, in the daytime, and at night (Table I; *P* values of pairwise comparisons are shown in Supplemental Fig. S12). Average RER can be compared between T-cycles because they have the same proportion of light and darkness.

Ws-2 grew more slowly in a T17 cycle than a T24 cycle ($p_t < 0.001$), and *lhycca1* grew more quickly in a T17 cycle than a T24 cycle ($p_t < 0.001$). Nevertheless, *lhycca1* in a T17 cycle still grew more slowly than Ws-2 in a T24 cycle ($p_t < 0.01$). Col-0 grew more slowly in a T28 cycle than a T24 cycle ($p_t < 0.001$), but *prr7prr9* grew only slightly and nonsignificantly faster in a T28 cycle than a T24 cycle ($p_t \geq 0.05$). It should be noted that, whereas in a T24 cycle, *lhycca1* grew much more slowly than Ws-2 ($p_t < 0.001$), *prr7prr9* was not significantly different from Col-0 ($p_t \geq 0.05$). Plant images (Supplemental Fig. S3) and estimated rosette areas (Supplemental Fig. S4A) reveal that *prr7prr9* was smaller than Col-0. The small size of *prr7prr9* might be due to slow growth before 17 DAS, when RER measurements started, or because the decrease in RER was too small to detect at a significant level.

We conclude that average RER increases in *lhycca1* and *prr7prr9* when they are grown in a T-cycle that matches their internal clock period but does not recover to the value found for the corresponding wild type in a T24 cycle. This is consistent with the idea that growth is decreased in these clock mutants by two factors: mismatch between the clock period and the external light-dark cycle as well as more direct effects on clock outputs.

Comparison of Average RER and the Rate of Deposition of C in Structural Biomass

In wild-type plants, average RER was higher in the night than in the daytime (Table I). For example, for Col-0, average RER is 92%, 50%, and 33% higher at night than in the light period in short (8-h), neutral (12-h), and long (16-h) photoperiods, respectively (Table I; Supplemental Fig. S13A). Growth was 33% faster in the night than in the daytime in Col-0 in a T28 cycle but not in Ws-2 in a T17 cycle. The relation between daytime and night growth was modified in clock mutants. In *prr7prr9*, preferential nighttime growth was even more marked (179% and 57% higher average RER at night than in the daytime in T24 and T28, respectively), whereas in *lhycca1*, average RER was higher in the daytime than at night (11% and 25% in T24 and T17 cycles, respectively).

Sulpice et al. (2014) used measurements of photosynthesis, respiration, starch, and other metabolites at dawn and dusk to estimate the average rate of C deposition in structural biomass in the light and dark periods, using Col-0 growing in similar conditions to this study. They found that the rate of synthesis of structural cellular components was 3- to 4-fold faster in the daytime than in the night in short and neutral photoperiods and slightly higher in the daytime than in the night in long photoperiods (summarized in Supplemental Fig. S13B). We compared the ratio of average RER in the night and the daytime in Col-0 with the ratio of the rate of synthesis of structural biomass in the night and the daytime (Fig. 6A). The dotted line indicates what would be expected if expansion growth and the synthesis of structural biomass occur in parallel. The estimated values lie below the line, showing that the synthesis of cellular components predominates in the daytime and expansion growth predominates at night. The discrepancy increases from a factor of 2 in LD to a factor of 10 in SD. We also multiplied average RER in the light and at night by the duration of the light period and night to calculate how much of the daily expansion growth occurs in the light period and the night. A similar calculation was performed for the synthesis of structural cellular components. As shown in Figure 6B, a larger proportion of the daily expansion growth occurs at night and a larger fraction of the

Table I. *Summary of the average rate of growth per hour in all genotypes and growth conditions over the whole light-dark cycle, in the light period, and in the night, comparison of the time shift between the maximum for RER and for the change in leaf angle, and amplitude of the change in leaf angle*

T-Cycle Categories	Photoperiod	Genotype and Treatment	RER[a] Whole Cycle	RER[a] Light (*, Subjected to DD)	RER[a] Dark (*, Subjected to LL)	Ratio Light to Dark	RER/h_{light}[b]	Time Shift[c]	Amplitude[d]
								h	°
T-cycle matches clock period	Neutral	Col-0_24	1.19 ± 0.15	0.97 ± 0.22	1.44 ± 0.18	0.67 ± 0.26	2.38 ± 0.30	+0.17	14.0
		Ws-2_24	1.25 ± 0.10	1.04 ± 0.16	1.49 ± 0.16	0.70 ± 0.19	2.50 ± 0.20	+0.17	15.7
		Ws-2_24(2)	1.27 ± 0.10	1.14 ± 0.22	1.45 ± 0.32	0.79 ± 0.29	2.54 ± 0.20	0.00	15.8
		Col-4_24	1.21 ± 0.10	1.16 ± 0.25	1.29 ± 0.17	0.90 ± 0.25	2.42 ± 0.20	−0.33	17.8
		*pif4pif5*_24	1.18 ± 0.10	1.10 ± 0.23	1.26 ± 0.24	0.87 ± 0.28	2.36 ± 0.20	−1.00	9.9
		*elf3*_24	1.19 ± 0.83	1.58 ± 1.48	0.87 ± 1.51	1.81 ± 1.76	2.38 ± 1.66	N.A.	5.1
		*lhycca1*_17	1.19 ± 0.11	1.30 ± 0.22	1.04 ± 0.22	1.25 ± 0.27	2.38 ± 0.22	−1.17	13.3
		*prr7prr9*_28	1.11 ± 0.13	0.83 ± 0.23	1.47 ± 0.21	0.56 ± 0.31	2.22 ± 0.26	−0.50	7.9
	Short	Col-0_SD	0.87 ± 0.13	0.56 ± 0.30	1.07 ± 0.16	0.52 ± 0.55	2.61 ± 0.26	−0.17	9.6
		Ws-2_SD	0.92 ± 0.10	0.83 ± 0.49	1.06 ± 0.28	0.78 ± 0.65	2.76 ± 0.20	−1.17 (5.00)	13.4
	Long	Col-0_LD	1.30 ± 0.14	1.24 ± 0.19	1.64 ± 0.33	0.75 ± 0.25	1.95 ± 0.28	−0.33	9.7
		Ws-2_LD	1.37 ± 0.15	1.29 ± 0.22	1.67 ± 0.32	0.77 ± 0.26	2.06 ± 0.30	−0.67	13.0
T-cycle longer than clock period	Neutral	*lhycca1*_24	1.09 ± 0.09	1.18 ± 0.19	1.06 ± 0.19	1.11 ± 0.24	2.18 ± 0.18	−1.33	7.7
		Col-0_28	1.07 ± 0.13	0.93 ± 0.17	1.24 ± 0.18	0.75 ± 0.23	2.14 ± 0.26	−1.83	7.4
T-cycle shorter than clock period	Neutral	*prr7prr9*_24	1.14 ± 0.17	0.62 ± 0.43	1.73 ± 0.38	0.36 ± 0.73	2.28 ± 0.34	+0.17	13.0
		Ws-2_17	1.18 ± 0.18	1.17 ± 0.40	1.18 ± 0.41	0.99 ± 0.49	2.36 ± 0.36	−0.33	14.5
Continuous	Light	Col-0_LL	1.09 ± 0.23	1.18 ± 0.22	1.01 ± 0.20*	1.17 ± 0.29	1.18 ± 0.22	−2.33	2.2
		Ws-2_LL	1.22 ± 0.36	1.45 ± 0.35	1.01 ± 0.18*	1.43 ± 0.30	1.45 ± 0.35	−1.50	8.6
	Dark	Col-0_DD	0.11 ± 0.28	0.21 ± 0.28*	0.09 ± 0.27	2.33 ± 3.28	–	–	–
		Ws-2_DD	0.10 ± 0.37	0.08 ± 0.40*	0.11 ± 0.34	0.73 ± 5.88	–	–	–

[a]Average RERs are calculated from the data in Figures 1 and 2 and Supplemental Figures S6 and S7, using all plants and all days in which the plants were imaged. Rates of growth are given as percentage per hour with means ± SD. The table also provides the ratio of RER in light and dark and the RER per hour of light (SD calculated with error propagation; i.e. 0.87/[8 h/24 h] = 2.61%/h_{light}) during the entire light-dark cycle for Col-0 in SD. The units of RER are $mm^2\ mm^{-2}\ h^{-1}$. [b][RER/(h light/h per cycle]. [c]Time shift that was required to maximize the correlation between RER and the change in hyponasty (h). The time shift of growth and hyponasty was studied using cross-correlation (Supplemental Fig. S18), with all mentioned correlations having significant *P* values ($P < 0.001$), and the amplitude of leaf angles are given. [d]Amplitude numbers, highest to lowest angle.

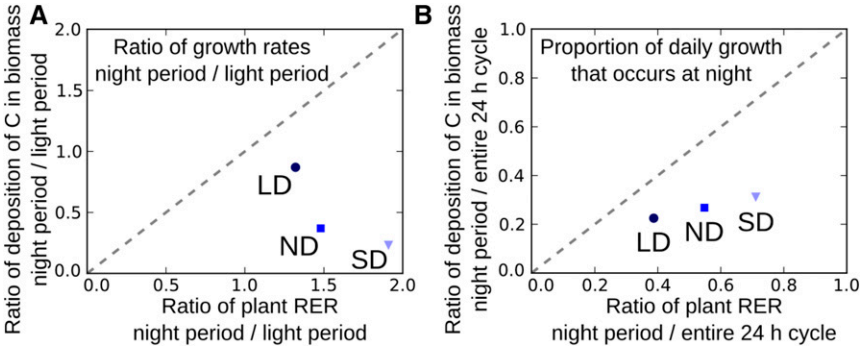

Figure 6. Comparison of the distribution of RER and the distribution of C deposition in structural biomass between the light period and night in wild-type Col-0 plants growing in different photoperiods. The data for RER are from Figures 1 and 2 and are summarized in Supplemental Figure S10A. The data for the deposition of C in structural biomass are from Sulpice et al. (2014), and the calculation and data are summarized in Supplemental Figure S13B. RER and C deposition in biomass are averaged across the night, the light period, or the entire 24-h cycle. A, Ratio of average RER in the light period and the night compared with the ratio of the rate of deposition of C in structural biomass in the light period and the night. Ratios are shown for Col-0 growing in LD (16- and 18-h photoperiods), neutral day (ND; 12-h photoperiod), and SD (8-h photoperiod) conditions. B, Proportion of the total daily RER and proportion of the total daily deposition of C in structural biomass that occurs at night in LD (16- and 18-h photoperiods), ND (12-h photoperiod), and SD (8-h photoperiod) conditions.

daily synthesis of structural biomass occurs in the light period, with the disproportion becoming larger in SD.

Hyponastic Leaf Movements

Diurnal changes of leaf angle in the various genotypes, T-cycles, and photoperiods and after transfer of wild-type plants to LL and DD are shown in Figures 7 and 8. The degree of similarity between the different treatments was analyzed by pairwise correlation of time series and by aligning data series with different T-cycles or photoperiods as described above for RER (Fig. 9A; Supplemental Fig. S14B). Transients early in the light and dark periods were compared by aligning the response to dawn and to dusk (Fig. 9, B and C; Supplemental Figs. S15 and S16).

The three wild types showed similar timing of hyponastic movement in a 12-h-light/12-h-dark cycle (Fig. 7, A and D). Leaf angle decreased after dawn to a minimum at about ZT2, recovered to a weak maximum at about ZT8 to ZT12, increased sharply about 1 h after dusk, increased further until about ZT20, and then decreased. Pairwise comparisons gave squared Pearson correlation coefficients (r^2) of 0.79, 0.95, and 0.87 between Col-0 and Ws-2, Col-0 and Col-4, and Col-4 and Ws-2, respectively (Fig. 9). As already seen for RER, leaf movement had a larger amplitude in Ws-2 than in Col-0 or Col-4 (Fig. 7, A and D).

We compared *lhycca1* and *prr7prr9* with the corresponding wild types. In *prr7prr9*, the rise in leaf angle in the light period was abolished and the decline at night was delayed compared with Col-0 (Fig. 7A). *lhycca1* showed a decrease in leaf angle after dawn and a rise after dusk, as in Ws-2 (Figs. 7B and 9B; Supplemental Fig. S16). However, leaf angle declined earlier in the night in *lhycca1* than in Ws-2. In addition, *lhycca1* showed a slight rise just before dawn rather than continuing to decline as in Ws-2. Leaf angles in *elf3* showed only a small decrease after dawn, a much weaker and delayed rise after dusk, and little or no decline at the end of the night (Fig. 7D). Compared with Col-4, *pif4pif5* showed a similar response in the light but a smaller increase in angle after dusk and generally smaller angles in the dark.

The small leaf angles in *pif4pif5* might be partly due to decreased petiole length preventing high angles (Lorrain et al., 2008; Dornbusch et al., 2014). Phenotyping^{4D} provides information about petiole length (Supplemental Fig. S17). There is no simple relationship between petiole length and the amplitude of the diurnal changes in leaf angle. *pif4pif5* had shorter petiole length and smaller hyponasty amplitudes than Col-4, Ws-2 had similar petiole length to Col-4 but higher amplitudes, and *elf3* had the longest petioles, a high leaf angle, with small amplitude.

We asked if the hyponasty phenotypes of *lhycca1* and *prr7prr9* are rescued by matching the clock period with the external light-dark cycle (Fig. 7B). *lhycca1* hyponasty was rescued in a T17 cycle, showing a very high correlation to Ws-2 in T24 (r^2 = 0.86). *prr7prr9* showed little or no change in a T28 cycle compared with a T24 cycle (r^2 = 0.89), in particular leaf angle remained low in the light (Fig. 7C). Col-0 and, to a lesser extent, *prr7prr9* showed a rise in angle before dawn in a T28 cycle. This resembled the rise before dawn in *lhycca1* in a T24 cycle or in *elf3* in a T24 cycle.

We also compared Col-0 and Ws-2 in different photoperiods (Fig. 7, E and F). The two accessions showed very similar timing of hyponastic responses in SD (r^2 = 0.83) and LD (r^2 = 0.92; the photoperiod data series were aligned on dawn and dusk [see above]). The amplitude of the hyponastic changes, including the rise in leaf angle after ZT2, was again larger in Ws-2 than in Col-0. In both accessions, the increase in leaf angle after ZT2 was more pronounced in longer photoperiods.

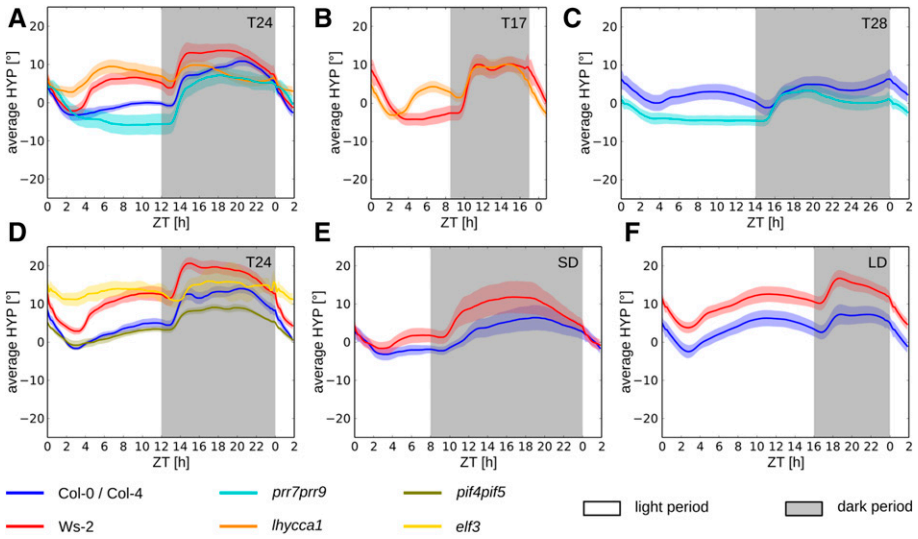

Figure 7. Diurnal hyponasty angles (HYP) of wild-type and mutant plants in different T-cycles and photoperiods. A, HYP of Col-0, Ws-2, *lhycca1*, and *prr7prr9* in a 12-h-light/12-h-dark cycle (T24). B, HYP of Ws-2 and *lhycca1* in an 8.5-h-light/8.5-h-dark cycle (T17). C, HYP of Col-0 and *prr7prr9* in a 14-h-light/14-h-dark cycle (T28). D, HYP of Col-4, Ws-2, *pif4pif5*, and *elf3* in a 12-h-light/12-h-dark cycle (T24). E, HYP of Col-0 and Ws-2 in an SD photoperiod with 8 h of light/16 h of dark (T24). F, HYP of Col-0 and Ws-2 in an LD photoperiod with 16 h of light/8 h of dark (T24). Diurnal changes in hyponasty were averaged for each plant over all sequential T-cycles, and means and SD were computed for $n \geq 10$ plants for each genotype, represented by lines and color-shaded areas, respectively, and a sliding median filter with a window of 1 h was applied. Time is given in hours after dawn (ZT). The data were collected from the same experiments as the RER determinations in Figures 1 and 2 and Supplemental Figure S9.

Irrespective of photoperiod duration, there was always a decrease in angle before and after dawn and a delayed increase in angle 1 to 4 h after dusk.

Hyponastic Movements of Wild-Type Plants in LL or DD

Hyponastic responses in Col-0 and Ws-2 were modified after transfer to free-running light (Fig. 8A). The transient decrease in angle after dawn and the increase in angle after dusk were abolished, and a smooth oscillation emerged with a peak toward the end of the subjective light period and a trough around subjective dawn. This resembles recent studies with Col-0 (Dornbusch et al., 2014; Greenham et al., 2015). The amplitude was larger in Ws-2 than in Col-0, matching the larger rise in leaf angle at ZT4 to ZT8 in a light-dark cycle in Ws-2 than in Col-0 (Fig. 7, A and D). The increased amplitude of leaf angle in Ws-2 is reminiscent of the large RER oscillation in Ws-2 (Fig. 3, A and B). After transfer to DD, the decrease in leaf angle at ZT2 was abolished and leaf angle instead rose strongly between ZT8 and ZT12 and then remained high (Fig. 8B).

Correlation-Based Cluster Analysis of Hyponasty across Genotypes and Treatments

A correlation-based cluster analysis for all neutral photoperiod treatments is presented in Figure 9A. Based on the silhouette scores (Supplemental Fig. S14A), we again selected six clusters. One cluster contained both Ws-2 data series (indicated in cyan; from the experiments of Fig. 1 and Supplemental Fig. S9) and was very closely related to a second cluster containing the other treatments in which genotypes were growing in a T-cycle that corresponded to their internal clock period (Col-0 and Col-4 in a T24 cycle, *pif4pif5* in a T24 cycle, and *lhycca1* in a T17 cycle; indicated in green). Within this cluster, *pif4pif5* grouped closely with the corresponding wild-type Col-4 and more loosely with Col-0. The third cluster contained plants growing in a T-cycle that was shorter than their internal circadian rhythm (Ws-2 in a T17 cycle and *prr7prr9* in a T24 cycle) as well as *prr7prr9* in T28 (indicated in black). Plants grown in a longer T-cycle than their internal clock period (Col-0 in a T28 cycle and *lhycca1* in a T24 cycle) lay outside the three main clusters. The cluster structure was retained in the analysis that included short- and long-photoperiod treatments (Supplemental Fig. S14B). Ws-2 and Col-0 in LD formed a new cluster, which showed some similarities to the large cluster with genotypes growing in a T-cycle that corresponded to their internal clock period. Ws-2 in SD was assigned to this large cluster. Col-0 in SD was assigned to the cluster that contained plants growing in a T-cycle that is longer than their internal circadian rhythm, possibly because the peak during the day was almost completely abolished (Fig. 7E), similar to Ws-2 in T17 (Fig. 7B).

Comparison of Changes in Leaf Angle after Dawn and after Dusk

In all genotypes, T-cycles, and photoperiods, there was a delayed rise in leaf angle after dusk (Fig. 7). We aligned the various leaf angle time series to dusk (Fig.

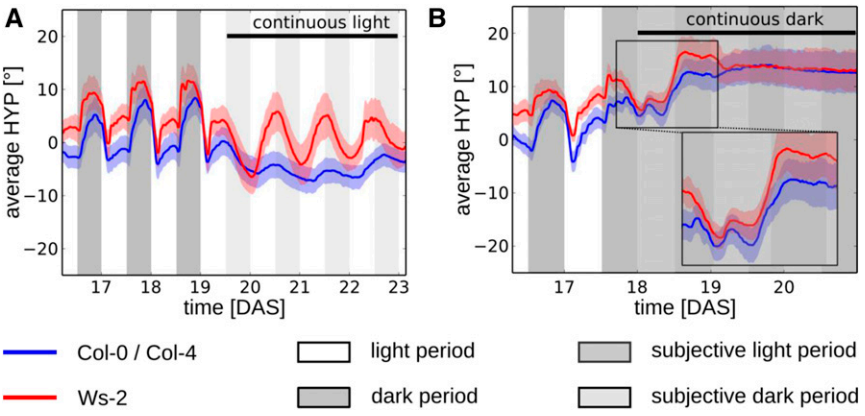

Figure 8. Hyponasty angles (HYP) of wild-type Col-0 and Ws-2 before and after the shift from a neutral-day T24 cycle to LL at 19 DAS or DD at 18 DAS. A, HYP before and after transfer of plants to LL. B, HYP before and after transfer of plants to DD. Lines and color-shaded areas represent means and SD, respectively ($n \geq 15$ plants for each genotype). Times are given as DAS.

9B; Supplemental Fig. S15A) and computed the first derivative of the leaf angle time series (Fig. 9C; Supplemental Fig. S15B). Averaged across all treatments, leaf angle started to increase 64 ± 19 min after dusk, and peak elevation rate was reached 111 ± 16 min after dusk. Closer inspection reveals that the time at which leaf angle started to increase was delayed slightly in Col-0 and Ws-2 in SD, in Col-0 in a T28 cycle, and in *elf3* in a T24 cycle (about 90, 80, 90, and 110 min after dusk, respectively; Supplemental Fig. S15). The time at which peak rates of elevation were reached also was delayed (about 230, 140, 140, and 150 min after dusk, respectively). However, these delays were small compared with the 4-h advance in short photoperiods, the 4-h delay in dusk in long photoperiods, and the 2-h delay in a T28 cycle (relative to the time elapsing between dawn and dusk in a neutral T24 cycle). The relatively consistent delay in upward movement in different T-cycles, photoperiods, and genotypes with different clock periods indicates that it represents a time-delayed response to darkening. In agreement, the rise was abolished in LL. Interestingly, leaf angle started to rise about 8 h after subjective dawn after transfer to DD (Fig. 8B). This indicates that the rise is triggered by darkening but gated by the clock, which suppresses it until ZT8, when the plant is left in the dark.

In all genotypes, T-cycles, and photoperiods, leaf angle decreased transiently and then recovered after dawn. Aligning the time series on dawn (Supplemental Fig. S16) revealed that this transient showed a similar timing in most treatments, with an average delay after dawn of 188 ± 37 min until the angle started to rise again. There was no consistent effect of a mismatch between the clock period and T-cycle duration. The delay was slightly shorter for *lhycca1* in a T24 cycle (140 min) and slightly longer for Col-0 in a T28 cycle (220 min) and for the two treatments where the T-cycle was shorter than their internal clock period (i.e. Ws-2 in a T17 cycle [240 min] and *prr7prr9* mutants in a T24 cycle [290 min]). Amplitude depended on the T-cycle; for example, it was typically smaller when the T-cycle was longer than the clock period (Table I; Fig. 7, A and C). Furthermore, amplitude was strongly attenuated in *elf3*. Overall, our results indicate that the transient changes in leaf angle after dawn and dusk are acute responses to light, but their amplitudes and in one case their timing may be modulated by the clock.

Temporal Interdependence of RER and Leaf Hyponasty

To investigate the temporal relationship between expansion growth and leaf movement, we first compared the correlation matrices for the RER and hyponasty time series (Figs. 4C and 9A). Correlations are much stronger in the hyponasty than in the RER data set, probably reflecting the lower noise in the hyponasty data set. The matrices show some similarities and some differences. In both matrices, the wild types in a T24 cycle are in one cluster and Ws-2 in T17, *prr7prr9* in T24, and *prr7prr9* in T28 are in a second cluster. However, treatments in which the T-cycle is longer than the clock period (Col-0 in a T28 cycle and *lhycca1* in a 24-h cycle) cluster together in the RER analysis but are strongly separated in the hyponasty analysis. Furthermore, *lhycca1* in T17 and *pif4pif5* in T24 cluster with wild-type T24 treatments in the hyponasty matrix but not in the RER matrix.

We also computed cross-correlation between the diurnal time series for RER and the leaf angle time series, varying the time shift between the two time series to identify the time shift (Δ) that maximizes the correlation (Table I; for an example, see Supplemental Fig. S18). We found no consistent temporal shift. In many cases, there was hardly any temporal displacement between RER and the change in leaf angle. In plants grown in a T-cycle longer than their circadian rhythm (e.g. Col-0 in T28 and *lhycca1* in T24), hyponastic movement was delayed by 1.8 and 1.3 h compared with RER, respectively. Comparison of the RER and hyponasty time series may be dominated by the large transient changes after dawn and dusk. We repeated the time-shift analysis using the time series from free-running light where these transients are absent (Supplemental Fig. S18, A and B). This revealed a delay between RER and change in leaf angle of 2.3 and 1.5 h for Col-0 and Ws-2,

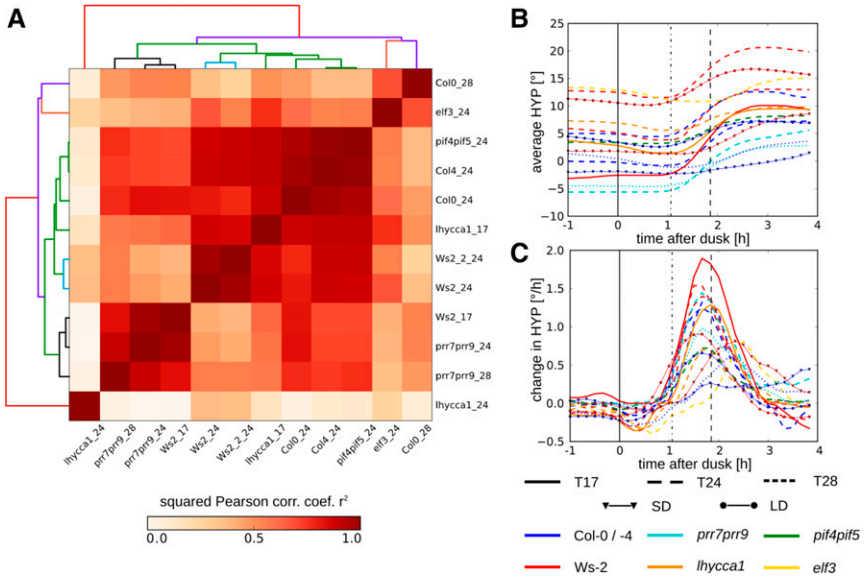

Figure 9. Correlation-based clustering of diurnal hyponasty angles (HYP) of wild-type and mutant plants in T24, T17, and T28 cycles in neutral-day conditions and alignment of HYP time series around dusk. A, Clustered heat map of all pairwise squared Pearson correlation coefficients (r^2) between rescaled hyponasty time series of different wild-type and mutant plants. For clustering analysis that also includes wild-type Col-0 and Ws-2 grown in SD and LD photoperiods, see Supplemental Figure S14. Ws2_24 and Ws2_2_24 refer to the Ws-2 data series in a 12-h-light/12-h-dark cycle in Figure 1B and Supplemental Figure S9B, respectively. Clustering was performed using hierarchical single-linkage clustering with a Euclidean distance measure. The number of clusters was determined using silhouette scores (Supplemental Fig. S14A), and the resulting clusters are color coded (1, red; 2, blue; 3, green; 4, black; 5, orange; 6, cyan). B, HYP aligned on dusk for all experiments, irrespective of the interval between dawn and dusk and the T-cycle duration. C, Change in HYP after dusk, given by the first derivative of the hyponasty time series. On average, leaf angle starts to increase 64 ± 19 min after dusk (vertical dashed-dotted line), with a maximum rate of change at 111 ± 16 min after dusk (vertical dashed line). Analogous analyses for the change in hyponasty at dawn are given in Supplemental Figure S16.

respectively. To investigate whether the analysis was sensitive to time averaging, we repeated the analysis using RER and leaf angle data that was time averaged over 3 h rather than 1 h. This yielded similar delays (2.2 and 1.7 h in Col-0 and Ws-2, respectively; Supplemental Fig. S18, C and D). We conclude that there is a delay of about 2 h between the circadian oscillations of RER and leaf angle but little or no time delay between the transients of RER and leaf angle after dawn and dusk.

Temporal Patterns of RER and Leaf Movement in Lower Red to Far-Red Light Regimes

Our experiments used a relative high ratio of red light to far-red light (R:FR) of 2.9. In two further experiments (Table I; Supplemental Fig. S19), we grew wild-type plants in R:FR of about 1, which is close to full natural sunlight (Smith, 1982), and 0.23, which is similar to deep shade and the conditions used by Dornbusch et al. (2014). Diurnal changes in RER at R:FR = 1 resembled those at R:FR = 2.9 (Fig. 1; Supplemental Table S1), including the transient inhibition after dawn and the transient stimulation after dusk (Supplemental Fig. S19A). Analyses of RER at R:FR of 0.23 were complicated by high leaf angle (Supplemental Fig. S8C) and by the long hypocotyl that led to plants occasionally tilting (Supplemental Fig. S19C). Hyponastic movement at R:FR of 1 and 0.23 resembled that at high R:FR, with a decrease and recovery after dawn and a delayed increase after dusk (Supplemental Fig. S19, B and D). To test if the analysis was sensitive to time averaging, we reanalyzed the R:FR = 0.23 leaf angle time series with time averaging over 3 h rather than 1 h (Supplemental Fig. S19E). The rise in leaf angle after dusk was still delayed by approximately 1 h.

DISCUSSION

Diurnal Changes in Leaf Expansion Growth in Wild-Type Arabidopsis in a T24 Cycle

The three wild types (Col-0, Col-4, and Ws-2) showed a qualitatively similar diurnal pattern in RER (Figs. 1–3; Supplemental Fig. S9) with four main features. The first was a slow oscillation with a peak at about ZT4 (Figs. 1 and 2) that was maintained in free-running light (Fig. 3). This oscillation was more marked in Ws-2. A similar oscillation in LL with a peak about 4 h after subjective dawn also was observed by Poiré et al. (2010) and Dornbusch et al. (2014). The second was a transient inhibition of expansion growth after dawn (Figs. 1 and 2; Supplemental Figs. S6 and S7). The third was a stimulation of expansion in the first 1 to 2 h after darkening (Figs. 1 and 2; Supplemental Figs. S6 and S9).

Both transients shifted with the timing of dusk in SD and LD (Fig. 2) and were modified or abolished after transfer to LL (Fig. 3), indicating that they are an acute response to light. Similar rapid transients were observed in some (Wiese et al., 2007; Dhondt et al., 2014) but not all (Dornbusch et al., 2014) previous studies (see also below). Fourth, average RER was higher in the night than in the light period (Fig. 1; Table I). This is not due to circadian regulation, as in LL average RER was not higher in the subjective night than in the subjective day (Fig. 3). Most of these features were seen in the clock mutants. However, average growth was faster in the daytime than at night in *lhycca1*, RER did not decrease early in the light period in *lhycca1*, and the decrease after dawn was stronger and more sustained in *prr7prr9*.

Mismatch between Clock Period and the External Light-Dark Cycle Leads to an Earlier and Stronger Inhibition of Leaf Expansion in the Last Hours of the Night

Another feature emerged in treatments in which the internal clock period differed from the external T-cycle. Two scenarios can be distinguished, depending on whether clock period was shorter or longer than the duration of the light-dark cycle. The decrease in RER at the end of the night started earlier and was stronger in Col-0 in a T28 cycle and in the short-period *lhycca1* mutant in a T24 cycle, and the premature decline in *lhycca1* was relieved when *lhycca1* was grown in a T17 cycle (Fig. 1). Correlation-based clustering of the diurnal RER response assigned Col-0 in a T28 cycle and *lhycca1* in a T24 cycle to the same cluster, distinctly separated from other treatments (Fig. 4). The inhibition of growth in the last hours of the night in treatments where clock period is shorter than the external light-dark cycle (*lhycca1* in T24 and wild-type Col-0 in T28) can be explained by premature exhaustion of starch. It is known that starch is prematurely exhausted in the short-period *lhycca1* mutant in a T24 cycle and in wild-type plants in a T28 cycle (Graf et al., 2010; Yazdanbakhsh et al., 2011; Scialdone et al., 2013). An abrupt decline of growth also is seen in wild-type plants when the night is suddenly extended, coinciding with the depletion of starch (Gibon et al., 2004; Usadel et al., 2008; Graf et al., 2010), and Dornbusch et al. (2014) showed that elongation growth resumes very rapidly after reillumination. A similar inhibition of root elongation in the last part of the night in *lhycca1* was rescued by supplying Suc (Yazdanbakhsh et al., 2011).

RER remained high until dawn when the internal clock period was longer than the external T-cycle in which the plants were grown; this response was observed for Ws-2 in a T17 cycle and *prr7prr9* in a T24 cycle (Fig. 1). Despite maintaining RER until dawn, the average RER over the whole night was decreased when the clock period was longer than the external light-dark cycle (Table I). Low average RER at night in Ws-2 in a T17 cycle might be explained because starch is incompletely mobilized in this short T-cycle (Graf et al., 2010). An analogous explanation might hold for *prr7prr9* in a 24-h cycle, but information about starch turnover in this mutant is needed to confirm this explanation. Ruts et al. (2012) showed that *CCA1*-overexpressing plants and especially the arrhythmic *prr5prr7prr9* triple mutant contain elevated starch levels at dawn compared with wild-type Col-0 and proposed that this could explain their lower rates of growth during the night. However, in these arrhythmic clock mutants, it is not possible to distinguish between responses to changes in period and to strongly perturbed clock function.

Taken together, these findings are consistent with a key role for the clock in pacing starch degradation to the length of the night to optimize the use of newly fixed C while avoiding deleterious periods of C starvation in the last part of the night.

The Growth Phenotype of *lhycca1* and *prr7prr9* Is Only Partly Complemented by Matching the Clock Period with the External Light-Dark Cycle

Dodd et al. (2005) reported that growth deficits in clock mutants with an altered clock period often can be reversed by matching the duration of the external light-dark cycle to the internal clock period, and Graf et al. (2010) proposed that this is partly because the clock paces starch turnover to the anticipated dawn. Our time-resolved studies reveal that many aspects of the growth phenotypes of clock mutants are not rescued by matching the external T-cycle to their clock period, pointing to further effects of the clock on extension growth.

Our results confirm that the short-period *lhycca1* mutant (Alabadí et al., 2002; Mizoguchi et al., 2002; Salomé and McClung, 2005) grows more slowly than the corresponding wild-type Ws-2 in a T24 cycle. The overall growth phenotype is partly but not completely rescued when *lhycca1* is grown in a short T-cycle (Fig. 1; Table I). The gain in growth in *lhycca1* in a T17 cycle compared with a T24 cycle was mainly due to a restoration of expansion growth at the end of the night. However, *lhycca1* commenced expansion growth after dawn more rapidly than wild-type Ws-2 in both a T24 cycle and a T17 cycle (Fig. 1). Furthermore, whereas wild-type plants showed higher average RER during the night than the day, *lhycca1* showed similar or faster expansion growth in the daytime than in the night even in a matching T17 cycle (Table I). The occurrence of a distinct growth phenotype in *lhycca1* that is unrelated to clock period length also is indicated by clustering, where *lhycca1* in a T17 cycle grouped separately from wild-type plants in a T-24 cycle (Fig. 4).

Compared with Col-0, the long-period *prr7prr9* mutant expanded faster during the night and maintains growth until the end of the night (Fig. 1). However, it showed a strong sustained inhibition of RER in the first part of the light cycle, and this daytime phenotype was not rescued in a T28 cycle (Fig. 1). Period length in

prr7prr9 has been reported to be as long as 32 h (Farré et al., 2005; Salomé and McClung, 2005) but is closer to 28 h when plants growing in the conditions used in our study are transferred to LL at growth irradiance (Flis et al., 2015). The occurrence of a distinct growth phenotype in *prr7prr9* that is not linked to the clock period length also is indicated by our correlation analysis, where *prr7prr9* in a T28 cycle clusters more closely to *prr7prr9* in a 24-h cycle than to treatments in which clock period matched T-cycle duration (Fig. 4).

lhycca1 is deficient in the dawn clock genes and shows early expression of day, dusk, and evening genes, whereas *prr7prr9* has high levels of *LHY* and *CCA1* transcript until the end of the light period and strongly delayed expression of dusk and evening genes (Pokhilko et al., 2012; Fogelmark and Troein, 2014; Flis et al., 2015). One possible explanation for the stimulation of expansion growth after dawn would be that *LHY* or *CCA1* restricts expansion growth at dawn and that this inhibition is relieved as the dawn components are repressed. The faster growth after dawn in *lhycca1* would be explained by the absence of the dawn component, and the stronger and more sustained inhibition of growth in *prr7prr9* might be explained by the continued expression of *LHY* and *CCA1* through the light period. Another explanation would be that the day genes act positively on expansion growth in the first part of the light period. Ruts et al. (2012) showed that expansion growth in the light is increased by overexpression of *CCA1* and also is increased relative to that in the night in *prr5prr7prr9*. This might indicate that *CCA1* and *LHY* act independently on expansion growth. However, interpretation of the response in *CCA1*-overexpressing lines and especially *prr5prr7prr9* is complicated because they are arrhythmic. Furthermore, any action of the dawn or day components might be direct or indirect via opposing action on the dusk or evening components.

Independent of these details, the interaction between the circadian clock and expansion growth in Arabidopsis rosettes differs from that in hypocotyls. First, the circadian peak is in the subjective light period. Second, as also pointed out by Dornbusch et al. (2014), whereas the evening complex inhibits hypocotyl extension in the middle of the T-cycle by repressing *PIF4* and *PIF5* (Nozue et al., 2007; Nusinow et al., 2011), in rosettes, the diurnal regulation of leaf elongation is affected only weakly in the *pif4pif5* mutant, and elongation in the middle of the T-cycle is inhibited rather than stimulated by the loss of *ELF3* function (Dornbusch et al., 2014).

Multiple Factors Inhibit Expansion Growth after Dawn and Stimulate Expansion Growth after Dusk

RER decreased transiently after dawn in almost all genotypes and treatments (Fig. 5). This decrease cannot be fully explained by circadian regulation. In LL, RER started to rise 2 to 4 h before subjective dawn in Ws-2 and just before subjective dawn in Col-0, where the oscillation was rather weak (Fig. 3). In a light-dark cycle, light and/or C signaling may modify these circadian oscillations, leading to a delay in the onset of expansion growth.

RER showed a strong transient stimulation after dusk in almost all investigated genotypes, T-cycles, and photoperiods (Figs. 1 and 2; Supplemental Figs. S6 and S9). The transient stimulation after dusk was independent of the duration of the light period (Fig. 2; Supplemental Fig. S9) and was abolished in LL (Fig. 3). These observations point to darkening leading to a transient stimulation of RER. A similar transient was observed in some (Wiese et al., 2007) but not all (Dornbusch et al., 2014) previous studies with Arabidopsis.

The transient inhibition of expansion growth after dawn and stimulation after dusk may be due partly to changes in leaf water deficit. Similar transients have been observed in many species, including monocots such as maize (*Zea mays*), wheat (*Triticum aestivum*), rice (*Oryza sativa*), and silvergrass (*Miscanthus* spp.) and dicots like sunflower (*Helianthus annuus*) and Arabidopsis (Boyer, 1968, 1988; Christ, 1978; Cutler et al., 1980; Clifton-Brown and Jones, 1999; Poiré et al., 2010). They have been attributed to evapotranspiration, leading to a decrease in xylem and leaf water potential in the light (Salah and Tardieu, 1997; Tang and Boyer, 2008; Ache et al., 2010; Pantin et al., 2011, 2012, 2013). Comparison of leaf size at successive dawns and dusks in Arabidopsis in different growth conditions and genotypes has provided evidence that the lower rate of expansion in the daytime compared with the night is related to a more negative leaf water deficit in the light (Pantin et al., 2011, 2012, 2013). Our higher temporal resolution indicates that much of this effect may be due to transient inhibition and stimulation of growth after illumination and darkening, respectively. The rates attained later in the light period and night are similar, pointing to the possibility that compensatory responses (Pantin et al., 2012) allow delayed adjustment of leaf expansion to changes in water deficit.

Relationship between Expansion Growth and the Synthesis of Structural Cell Components

Leaf growth requires two interlocking processes: (1) cell expansion due to water uptake into the vacuole, which is driven by water status, cellular osmolarity, and increased cell wall extensibility (Carpita and Gibeaut, 1993; Gonzalez et al., 2012; Pantin et al., 2012); and (2) synthesis of cell wall, protein, and other structural components. These will interact to determine final leaf size, protein concentration, and cell wall thickness. These are important attributes for leaf function and are modified in response to environmental conditions (Poorter and Nagel, 2000; Poorter et al., 2009).

As already mentioned, expansion growth is faster in the night than during the light period (Table I; Supplemental Fig. S13). This contrasts with structural cellular components, which are synthesized faster in the

light period than in the night. The latter was shown by whole-plant C balance modeling, using measurements of photosynthesis, respiration, and starch and metabolite levels, and confirmed by analyses of polysome loading as a qualitative proxy for the rate of protein synthesis (Pal et al., 2013; Sulpice et al., 2014) and by performing dynamic $^{13}CO_2$ labeling to measure absolute rates of protein and cell wall synthesis (Ishihara et al., 2015). Temporal uncoupling of expansion growth and the synthesis of cellular components is relatively small (about 2-fold) in long photoperiods and becomes larger (up to 10-fold) as the photoperiod is shortened (Fig. 6).

Preferential expansion at night and the synthesis of structural components in the light may reflect their differing dependence on energy, C, and water. Expansion growth may be more dependent on the water status, which is likely to be more favorable in the dark (Pantin et al., 2012), whereas the synthesis of structural cellular components is strongly dependent on energy and C, which are more readily available in the light, especially in short photoperiods. Ruts et al. (2012) proposed that the low rates of expansion of *CCA1*-overexpressing plants and especially the arrhythmic *prr5prr7prr9* triple mutant during the night might be due to the incomplete mobilization of starch. It is possible, however, that the incomplete mobilization of starch in these arrhythmic mutants is due to lower demand due to decreased growth at night. Interactions between resources may be further modified by environmental and physiological signals and developmental responses. Structural biomass decreases relative to leaf area in low light or in mutants with decreased rates of photosynthesis (Boardman, 1977; Fichtner et al., 1993; Tardieu et al., 1999), including Arabidopsis (Cookson and Granier, 2006; Pantin et al., 2011). C starvation limits leaf expansion in the night in the starchless *pgm* mutant (Wiese et al., 2007; Apelt et al., 2015), and application of GA_3 rescues expansion but not the synthesis of structural biomass (Paparelli et al., 2013). Furthermore, the growth of very young leaves, which is primarily due to cell division, is faster in the night and more dependent on the C supply, whereas the growth of larger leaves, which is mainly due to cell expansion, is faster in the night (Pantin et al., 2011, 2012, 2013). These findings raise questions about how these temporally and spatially separated processes are coordinated over a longer time frame to regulate final leaf size and composition. Integration of information by the clock about the environment and the physiological status at checkpoints such as dusk and dawn may play an important role in this coordination.

Clock and Light Signaling Affect Hyponastic Movement

Hyponastic leaf movement in Arabidopsis is thought to depend on uneven cell expansion rates in the abaxial and adaxial parts of the petiole (see introduction). Diurnal changes in hyponasty and RER (Figs. 1, 2, and 7; Supplemental Figs. S6 and S9) exhibit three similarities: (1) a slow oscillation that is maintained in LL; (2) a rapid decrease in RER and leaf angle after dawn; and (3) a delayed marked increase in RER and leaf angle after dusk. Furthermore, higher average RER in the night coincides with a higher average leaf angle.

Comparison of the various mutants and light regimes provides insights into how the clock interacts with other inputs to regulate leaf orientation. Leaf angle in wild-type Col-0 and Ws-2 shows a slow oscillation in LL, with a peak rate of increase about 6 h after subjective dawn and a maximum angle about 10 to 12 h after subjective dawn (Fig. 8). A similar circadian oscillation was reported for Col-0 by Dornbusch et al. (2014). Like the oscillation in RER, the amplitude of oscillation in leaf angle was more pronounced in Ws-2 than in Col-0. The impact of this circadian oscillation can be seen clearly in light-dark cycles (Fig. 7), including the more pronounced rise of leaf angle from ZT3 onward in Ws-2 than in Col-0, the earlier decline in the light period in the short-period *lhycca1* mutant in a T24 cycle, and the rise in leaf angle before dawn in Col-0 in a T28 cycle and in *lhycca1* in a T24 cycle. Furthermore, the peak of the endogenous oscillation at about 10 to 12 h after subjective dawn in a free-running light cycle (Fig. 8) corresponds to when leaf angle peaks in a 12- or 16-h photoperiod for Ws-2 and Col-0 in a T24 cycle and for Col-0 in a T28 cycle (Fig. 7).

The amplitude of hyponastic movement was smaller in *prr7prr9*. This might be due, in principle, to one of three factors: (1) the endogenous oscillation in leaf angle is driven by *PRR7* and/or *PRR9*; (2) the oscillation is suppressed by *LHY* and/or *CCA1*, whose expression remains high for most of the light period in *prr7prr9* (see above); or (3) the oscillation depends on dusk and evening components, whose rise is delayed in *prr7prr9* (see above). A major role for *LHY* and *CCA1* appears unlikely, because the changes in leaf angle at day were similar in *lhycca1* and wild-type Ws-2, except for a slight delay of the former, which can be explained by the short period of this mutant. Furthermore, the hyponastic phenotype of *lhycca1* in a T17 cycle showed a very high correlation to that of Ws-2 in a T24 cycle ($r^2 = 0.86$) and clustered with wild types in a T24 cycle. In contrast, the hyponasty phenotype of the *prr7prr9* mutant in a T28 cycle did not correlate well with Col-0 in a T24 cycle and, instead, clustered most closely with *prr7prr9* in a T24 cycle. These results point to the involvement of day clock components in the increase in leaf angle during the light period.

A role for *ELF3* in promoting the increase in leaf angle from ZT3 onward seems unlikely, as *elf3* showed a high angle throughout the 24-h cycle both in our study (Fig. 7) and previously (Dornbusch et al., 2014). As *ELF3* plays a key role in the integration of light signals (Zagotta et al., 1996; Dowson-Day and Millar, 1999; Niwa et al., 2009), it is possible that the high and rather constant leaf angle might be due to the attenuation of light responses rather than to the loss of a clock output. Nevertheless, there was still a small decrease in angle

after dawn and an increase after dusk in *elf3* (Supplemental Fig. S16), indicating that irradiance still affects leaf angle in the absence of ELF3 function.

Leaf angle decreased in the first hour after dawn in all genotypes and conditions (Fig. 7; Supplemental Fig. S16). This coincided with the timing of the endogenous oscillation in LL, which was at a minimum at about subjective dawn, but the decline was accentuated in light-dark cycles. Furthermore, while the endogenous oscillation was stronger in Ws-2 than in Col-0 (see above), the transient decline after dawn was similar in both wild types. Also, the kinetics and amplitude of the decline were not modified in a consistent manner by a mismatch between clock period and the external T-cycle. Thus, while low leaf angle at dawn may be due partly to circadian regulation, it is accentuated by light.

Another dominant feature of the diurnal hyponastic response was a delayed rise in angle after dusk, starting about 1 h and reaching a maximum rate of increase about 1.6 h after dusk (Fig. 9; Supplemental Fig. S15). While this rise was abolished in LL, an increase in leaf angle was seen in DD, starting approximately 8 h and being completed approximately 14 h after subjective dawn (Fig. 8). These observations are consistent with the idea that the increase in leaf angle is a response to a light-dark transition but is gated by the clock such that it cannot occur until about 8 to 9 h after dawn. In agreement, the rise after dusk was delayed slightly in Ws-2 and Col-0 in an 8-h photoperiod (Supplemental Fig. S15). It is interesting that the proposed time interval during which the clock prevents a dark-dependent increase in leaf angle corresponds to the time at which the rise in leaf angle starts to slow down in a free-running light cycle and the time at which the leaf angle peaks in the light period in wild-type plants in a 12- or 16-h photoperiod.

Transient changes of leaf angle after dawn and dusk were detected in several Arabidopsis accessions by Bours et al. (2012), who used the apparent distance between the rosette center and leaf tips in a 2D image as an approximation for leaf movement. While there were transients in leaf angle after dawn and after dusk previously (Dornbusch et al., 2014), they were less marked than in our study. Dornbusch et al. (2014) used a low R:FR similar to shade light, whereas we used a high R:FR for most of the experiments. We observed similar transients at low R:FR, but they became less obvious when we applied a 3-h moving average similar to that used by Dornbusch et al. (2014; Supplemental Fig. S19). Indirect evidence for the involvement of phytochrome signaling is provided by the decreased amplitude of leaf movement after dawn and dusk in the *pif4pif5* mutant, both in our study (Fig. 7) and previously (Dornbusch et al., 2014).

Relation between Diurnal Changes in RER and Leaf Movement

Comparison of the timing of leaf expansion growth and leaf movement is complicated because both responses involve an interaction between an endogenous oscillation and transient changes after dawn and dusk. When only the oscillations in free-running light are considered, there is a delay of 1.5 h in Ws-2 and 2.3 h in Col-0 between changes in RER and leaf angle (Table I; Supplemental Fig. S18). This is not dissimilar to the 3-h delay estimated by Dornbusch et al. (2014). In contrast, the transient responses of RER and leaf movement after dawn and dusk do not show a marked or consistent time offset (Table I). Irrespective of the reason for these transients, the contrasting temporal relationship between RER and leaf movement in the circadian oscillation and the transients make it unlikely that there is a direct causal relationship and indicate that the time offset in the endogenous oscillation is more likely to be due to differences in the timing of the upstream clock output.

CONCLUSION

In conclusion, both leaf expansion growth and hyponastic leaf movement show strong diurnal changes that are driven by a circadian oscillation, overlaid by large transient changes after dawn and dusk that are probably due to direct or indirect responses to light, including changes in water status. The circadian peak in expansion at about ZT4 may be due to positive regulation by day clock components or recovery from inhibition by dawn components. In addition to driving an endogenous oscillation in RER, the clock paces starch breakdown to avoid transient starvation and the inhibition of growth at the end of the night. The endogenous oscillation in expansion growth is strongly modified by the light-dependent transients after dawn and dusk. Furthermore, expansion growth is faster in the night, whereas the synthesis of cellular components is faster in the light period. This may reflect the differing dependence of these processes on energy, C, and water. The circadian oscillation plays a more visible role in hyponastic movements in light-dark cycles, and day clock components may play a major role in promoting an increase in leaf angle during the first part of the T-cycle.

MATERIALS AND METHODS

Plant Material

Arabidopsis (*Arabidopsis thaliana*) accessions Col-0, Col-4, and Ws-2 were obtained from the institute seed stock (Dr. Karin Köhl, Max Planck Institute of Molecular Plant Physiology). Clock mutants *prr7.3/prr9.1* (Salomé and McClung, 2005), *lhy.11/cca1.21* (Hall et al., 2003), and *elf3.4* (Zagotta et al., 1996) were provided by Andrew Millar (University of Edinburgh). *pif4pif5* was provided by Karen Halliday (University of Edinburgh).

Experimental Setup and Imaging System

Arabidopsis accessions were grown in 10-cm-diameter pots filled with soil and soaked overnight in water containing fungicide and boric acid solution. In each pot, four equidistant spots were initially sown with 10 to 20 seeds per spot. The seeds were germinated in a growth chamber (model E-36L; Percival Scientific; http://www.percival-scientific.com/) under a 12-h-light (photosynthetically active

radiation of 160 μmol m^{-2} s^{-1} at the plant level) and 12-h-dark (20°C and 18°C, respectively) cycle. One week after sowing, plants were thinned to one plant per spot. Before imaging, the soil surface was covered with black plastic-coated quartz sand (approximately 0.5 mm diameter) to reduce near-infrared light reflection. Plants were imaged typically from 17 to 24 DAS.

The light-field camera image system is part of Phytotyping^{4D}, a fully automated, noninvasive, and accurate light-field camera-based imaging system (Apelt et al., 2015). It employs a light-field camera (R29; Raytrix; http://www.raytrix.de/; Perwass and Wietzke, 2012) mounted with a 100-mm lens (Makro-Planar T* 2/100; Zeiss; http://www.zeiss.de/) with an effective focal length of 155 mm and an 850-nm longpass filter. Up to 12 pots, of 10 cm diameter, each containing four plants, were mounted on a robotic cross stage with a travel range of 450 × 390 mm (KS15; ITK Dr. Kassen; http://www.itknet.com/) located in a controlled growth chamber and illuminated additionally with near-infrared light-emitting diodes (TV6816; ABUS; http://www.abus.com/) with an emission spectrum of 820- to 1,050 nm that is detected by the camera sensor but does not interfere with plant growth (Kelly and Lagarias, 1985). A daylight cutoff filter (850-nm longpass filter) ensures equivalent image exposure during the day and the night. The setup enables a time resolution of five images per hour per plant. The camera was initially calibrated using RxLive software (version 2.8; Raytrix) to detect microlens positions and devignette the microlens images. For each recording, it simultaneously provides a focus image (PNG image; 3,288 × 2,192 pixels, eight-bit depth, 2.9 MB) and a depth image (PNG image; 3,288 × 2,192 pixels, 16-bit depth, 6.6 MB) from which the 3D surface of the recorded plant may be reconstructed (Supplemental Fig. S1). Parameters for the computation of the metric depth information from the grayscale depth images were determined using printed discs of known sizes as well as a real plant imaged under different angles (Apelt et al., 2015). In our experimental setup, the spatial resolution of the camera is more than 35 pixels mm^{-1}.

Automated Image Analysis of Plant Growth and Leaf Movement

Phytotyping^{4D} employs an automated image-processing pipeline that accurately segments a given plant from the soil background and computes various biologically relevant features of plant growth behavior. Detailed definitions and descriptions can be found in Supplemental Methods S1 and Apelt et al. (2015). By combining light-field camera-based focus and depth images, the pipeline measures plant 3D surface areas via triangulation. From the segmented plants and their 3D areas, their RERs are derived. By further segmenting individual leaves of a given plant, the average leaf area-weighted angle between the leaf base and tip is computed as a measure for leaf hyponasty.

To enable robust statistical analyses, at least 12 plants per studied genotype and condition were imaged. To avoid artifacts from plants with severe growth defects, outliers were excluded. To this end, for a given genotype and condition, we computed the diurnal RER time series for all plants and performed a principal component analysis (PCA) on these time series (Jolliffe, 2002). For the first two principal components, we computed the average, or center, and SD across plants and excluded plants lying more than 2 SD from the center. We then performed a second PCA-based filtering to remove further outliers whose RERs differed in features not resolved by principal components of the first PCA. All diurnal RERs and hyponastic patterns were calculated with a sliding median of 1 h.

Statistical Analyses

RER and leaf angle data are shown as means ± SD, calculated from n ($n > 10$) individual plants. To test for differences between the diurnal RERs, we applied independent, equal-variance Student's t tests to single time points as well as over 1-h sliding windows, where unsmoothed RERs of different plants were considered separately (Figs. 1 and 2; Supplemental Figs. S7 and S9). Differences between average growth rates per cycle, per light period, or per night also were determined using independent, equal-variance Student's t tests (Supplemental Fig. S12).

Clustering of RER and hyponasty time series (Figs. 4C and 9A; Supplemental Figs. S11 and S14) was performed on the pairwise Pearson correlation matrix of the time series, whereby high correlation coefficients indicate high similarity of the two time series. To compare time series RER and hyponasty angles across different genotypes, T-cycles, and photoperiods, the diurnal time series were aligned at dawn (to align different T-cycles) or at dawn and at dusk (for different photoperiods, equidistant data points of the longer periods were deleted to match the length of the shorter period), enabling the calculation of Pearson correlation coefficients (Fig. 4B). The resulting correlation matrix was clustered using hierarchical single-linkage clustering with a Euclidean distance measure (Fig. 4C). Cluster quality was measured using silhouette scores (Rousseeuw, 1987), and the highest number of clusters before a steep decline in the silhouette score was selected for clustering (Supplemental Figs. S11 and S14; Rousseeuw, 1987).

Discrete Fourier transformation was used to detect the dominant oscillation frequency in RER time series of Col-0 and Ws-2 wild-type plants grown in LL, indicated by the peak amplitude in the Fourier spectrum (Fig. 3, C and D). To quantify the nonrandomness of this oscillation, we shuffled the RER data 100 times and recomputed the Fourier spectrum for each randomized time series. A z-score was used to measure the distance between the Fourier peak amplitude of the biological data and the amplitude at the corresponding oscillation period of the randomized data.

Accession Numbers

Sequence data from genes studied in this article can be found in the GenBank/EMBL data libraries under the following gene identifier codes: At5g02810 (PRR7), At2g46790 (PRR9), At1g01060 (LHY), At2g46830 (CCA1), At2g43010 (PIF4), At3g59060 (PIF5), At2g25930 (ELF3).

Supplemental Data

The following supplemental materials are available.

Supplemental Figure S1. Simplified clock model.

Supplemental Figure S2. Representative image data from Phytotyping^{4D} comprising a focus image and a depth image from which the 3D surface of the plant may be reconstructed.

Supplemental Figure S3. Light-field camera focus images of Arabidopsis wild-type and mutant plants.

Supplemental Figure S4. Increase in total plant 3D surface area over time for wild-type and mutant plants under different conditions.

Supplemental Figure S5. Analysis of the origins of SD in time series of growth rates and leaf hyponasty angles and heat maps of individual diurnal RER and diurnal hyponastic patterns for an example experiment.

Supplemental Figure S6. Diurnal RER and diurnal hyponastic pattern for individual plants in all experiments.

Supplemental Figure S7. Diurnal RER, Student's t test results, and two-way ANOVA results for unsmoothed data.

Supplemental Figure S8. Heat maps indicating the proportion of the rosette at different angles for Col-0, Ws-2, and *elf3* under standard growth conditions and Ws-2 under low R:FR.

Supplemental Figure S9. Diurnal RER of wild-type and *elf3* and *pif4pif5* mutant plants in a T24 cycle in neutral-day conditions.

Supplemental Figure S10. Dawn alignment of RER time series in the second part of the night to allow comparison of predawn RER in different genotypes and T-cycles

Supplemental Figure S11. Silhouette plots for clustering of RER treatments, and clustered heat map of all rescaled RER time series for all performed experiments, including short and long photoperiods.

Supplemental Figure S12. Testing for the significance of differences in average RER during the light period, the dark period, and the complete diurnal cycle via pairwise testing (independent two-sample Student's t test P values).

Supplemental Figure S13. Comparison of the distribution of expansion growth and the distribution of C deposition in structural biomass in wild-type Col-0 growing in different photoperiods.

Supplemental Figure S14. Silhouette plots for clustering of RER and clustered heat map of rescaled hyponasty time series of all performed experiments, including short and long photoperiods.

Supplemental Figure S15. Hyponasty angle and change in hyponasty angle after dusk for wild-type plants in short, neutral, and long photoperiods.

Supplemental Figure S16. Hyponasty angle and change in hyponasty angle at the start of the light period, aligned to dawn.

Supplemental Figure S17. Dependence of hyponasty amplitude on petiole length of different wild-type and mutant plants under different conditions.

Supplemental Figure S18. Cross-correlation analysis of growth rates and changes in leaf hyponasty angle in wild-type Col-0 and Ws-2 after transfer to LL and comparison of different methods for smoothing of the time series.

Supplemental Figure S19. Diurnal changes in RER and leaf angle in light regimes with R:FR of 1 and 0.23.

Supplemental Table S1. Overview of experiments.

Supplemental Methods S1. Automated image analysis of plant growth and leaf movement.

Received April 12, 2017; accepted May 16, 2017; published May 30, 2017.

LITERATURE CITED

Ache P, Bauer H, Kollist H, Al-Rasheid KA, Lautner S, Hartung W, Hedrich R (2010) Stomatal action directly feeds back on leaf turgor: new insights into the regulation of the plant water status from non-invasive pressure probe measurements. Plant J **62:** 1072–1082

Adams S, Manfield I, Stockley P, Carré IA (2015) Revised morning loops of the Arabidopsis circadian clock based on analyses of direct regulatory interactions. PLoS ONE **10:** e0143943

Alabadí D, Yanovsky MJ, Más P, Harmer SL, Kay SA (2002) Critical role for CCA1 and LHY in maintaining circadian rhythmicity in Arabidopsis. Curr Biol **12:** 757–761

Apelt F, Breuer D, Nikoloski Z, Stitt M, Kragler F (2015) Phytotyping^{4D}: a light-field imaging system for non-invasive and accurate monitoring of spatio-temporal plant growth. Plant J **82:** 693–706

Boardman N (1977) Comparative photosynthesis of sun and shade plants. Annu Rev Plant Physiol **28:** 355–377

Bours R, Muthuraman M, Bouwmeester H, van der Krol A (2012) OSCILLATOR: a system for analysis of diurnal leaf growth using infrared photography combined with wavelet transformation. Plant Methods **8:** 29

Boyer JS (1968) Relationship of water potential to growth of leaves. Plant Physiol **43:** 1056–1062

Boyer JS (1988) Cell enlargement and growth-induced water potentials. Physiol Plant **73:** 311–316

Carpita NC, Gibeaut DM (1993) Structural models of primary cell walls in flowering plants: consistency of molecular structure with the physical properties of the walls during growth. Plant J **3:** 1–30

Carré I, Veflingstad SR (2013) Emerging design principles in the Arabidopsis circadian clock. Semin Cell Dev Biol **24:** 393–398

Christ R (1978) The elongation rate of wheat leaves. II. Effect of sudden light change on the elongation rate. J Exp Bot **29:** 611–618

Clifton-Brown J, Jones M (1999) Alteration of transpiration rate, by changing air vapour pressure deficit, influences leaf extension rate transiently in Miscanthus. J Exp Bot **50:** 1393–1401

Cookson SJ, Granier C (2006) A dynamic analysis of the shade-induced plasticity in Arabidopsis thaliana rosette leaf development reveals new components of the shade-adaptative response. Ann Bot (Lond) **97:** 443–452

Cutler JM, Steponkus PL, Wach MJ, Shahan KW (1980) Dynamic aspects and enhancement of leaf elongation in rice. Plant Physiol **66:** 147–152

Dhondt S, Gonzalez N, Blomme J, De Milde L, Van Daele T, Van Akoleyen D, Storme V, Coppens F, Beemster GTS, Inzé D (2014) High-resolution time-resolved imaging of in vitro Arabidopsis rosette growth. Plant J **80:** 172–184

Dodd AN, Salathia N, Hall A, Kévei E, Tóth R, Nagy F, Hibberd JM, Millar AJ, Webb AAR (2005) Plant circadian clocks increase photosynthesis, growth, survival, and competitive advantage. Science **309:** 630–633

Dornbusch T, Lorrain S, Kuznetsov D, Fortier A, Liechti R, Xenarios I, Fankhauser C (2012) Measuring the diurnal pattern of leaf hyponasty and growth in Arabidopsis: a novel phenotyping approach using laser scanning. Funct Plant Biol **39:** 860–869

Dornbusch T, Michaud O, Xenarios I, Fankhauser C (2014) Differentially phased leaf growth and movements in *Arabidopsis* depend on coordinated circadian and light regulation. Plant Cell **26:** 3911–3921

Dowson-Day MJ, Millar AJ (1999) Circadian dysfunction causes aberrant hypocotyl elongation patterns in Arabidopsis. Plant J **17:** 63–71

Farré EM (2012) The regulation of plant growth by the circadian clock. Plant Biol (Stuttg) **14:** 401–410

Farré EM, Harmer SL, Harmon FG, Yanovsky MJ, Kay SA (2005) Overlapping and distinct roles of PRR7 and PRR9 in the Arabidopsis circadian clock. Curr Biol **15:** 47–54

Fichtner K, Quick W, Schulze ED, Mooney H, Rodermel S, Bogorad L, Stitt M (1993) Decreased ribulose-1,5-bisphosphate carboxylase-oxygenase in transgenic tobacco transformed with "antisense" rbcS. Planta **190:** 1–9

Flis A, Fernández AP, Zielinski T, Mengin V, Sulpice R, Stratford K, Hume A, Pokhilko A, Southern MM, Seaton DD, et al (2015) Defining the robust behaviour of the plant clock gene circuit with absolute RNA timeseries and open infrastructure. Open Biol **5:** 150042

Flis A, Sulpice R, Seaton DD, Ivakov AA, Liput M, Abel C, Millar AJ, Stitt M (2016) Photoperiod-dependent changes in the phase of core clock transcripts and global transcriptional outputs at dawn and dusk in Arabidopsis. Plant Cell Environ **39:** 1955–1981

Fogelmark K, Troein C (2014) Rethinking transcriptional activation in the Arabidopsis circadian clock. PLOS Comput Biol **10:** e1003705

Gibon Y, Bläsing OE, Palacios-Rojas N, Pankovic D, Hendriks JHM, Fisahn J, Höhne M, Günther M, Stitt M (2004) Adjustment of diurnal starch turnover to short days: depletion of sugar during the night leads to a temporary inhibition of carbohydrate utilization, accumulation of sugars and post-translational activation of ADP-glucose pyrophosphorylase in the following light period. Plant J **39:** 847–862

Gibon Y, Pyl ET, Sulpice R, Lunn JE, Höhne M, Günther M, Stitt M (2009) Adjustment of growth, starch turnover, protein content and central metabolism to a decrease of the carbon supply when Arabidopsis is grown in very short photoperiods. Plant Cell Environ **32:** 859–874

Gonzalez N, Vanhaeren H, Inzé D (2012) Leaf size control: complex coordination of cell division and expansion. Trends Plant Sci **17:** 332–340

Graf A, Schlereth A, Stitt M, Smith AM (2010) Circadian control of carbohydrate availability for growth in Arabidopsis plants at night. Proc Natl Acad Sci USA **107:** 9458–9463

Graf A, Smith AM (2011) Starch and the clock: the dark side of plant productivity. Trends Plant Sci **16:** 169–175

Greenham K, Lou P, Remsen SE, Farid H, McClung CR (2015) TRiP: Tracking Rhythms in Plants, an automated leaf movement analysis program for circadian period estimation. Plant Methods **11:** 33

Hädrich N, Hendriks JHM, Kötting O, Arrivault S, Feil R, Zeeman SC, Gibon Y, Schulze WX, Stitt M, Lunn JE (2012) Mutagenesis of cysteine 81 prevents dimerization of the APS1 subunit of ADP-glucose pyrophosphorylase and alters diurnal starch turnover in Arabidopsis thaliana leaves. Plant J **70:** 231–242

Hall A, Bastow RM, Davis SJ, Hanano S, McWatters HG, Hibberd V, Doyle MR, Sung S, Halliday KJ, Amasino RM, et al (2003) The TIME FOR COFFEE gene maintains the amplitude and timing of *Arabidopsis* circadian clocks. Plant Cell **15:** 2719–2729

Harmer SL, Hogenesch JB, Straume M, Chang HS, Han B, Zhu T, Wang X, Kreps JA, Kay SA (2000) Orchestrated transcription of key pathways in Arabidopsis by the circadian clock. Science **290:** 2110–2113

Ishihara H, Obata T, Sulpice R, Alisdair RF, Stitt M (2015) Quantifying protein synthesis and degradation in Arabidopsis by dynamic 13CO2 labeling and analysis of enrichment in individual amino acids in their free pools and in protein. Plant Physiol **168:** 74–93

Izumi M, Hidema J, Makino A, Ishida H (2013) Autophagy contributes to nighttime energy availability for growth in Arabidopsis. Plant Physiol **161:** 1682–1693

Jolliffe I (2002) Principal component analysis. Wiley Online Library, doi/10.1002/0470013192.bsa501

Kamioka M, Takao S, Suzuki T, Taki K, Higashiyama T, Kinoshita T, Nakamichi N (2016) Direct repression of evening genes by CIRCADIAN CLOCK-ASSOCIATED1 in the *Arabidopsis* circadian clock. Plant Cell **28:** 696–711

Kelly JM, Lagarias JC (1985) Photochemistry of 124-kilodalton Avena phytochrome under constant illumination in vitro. Biochemistry **24:** 6003–6010

Lorrain S, Allen T, Duek PD, Whitelam GC, Fankhauser C (2008) Phytochrome-mediated inhibition of shade avoidance involves degradation of growth-promoting bHLH transcription factors. Plant J **53:** 312–323

Lu Y, Gehan JP, Sharkey TD (2005) Daylength and circadian effects on starch degradation and maltose metabolism. Plant Physiol **138:** 2280–2291

Michael TP, Mockler TC, Breton G, McEntee C, Byer A, Trout JD, Hazen SP, Shen R, Priest HD, Sullivan CM, et al (2008) Network discovery pipeline elucidates conserved time-of-day-specific cis-regulatory modules. PLoS Genet **4:** e14

Mizoguchi T, Wheatley K, Hanzawa Y, Wright L, Mizoguchi M, Song HR, Carré IA, Coupland G (2002) LHY and CCA1 are partially redundant genes required to maintain circadian rhythms in Arabidopsis. Dev Cell **2:** 629–641

Nakamichi N (2011) Molecular mechanisms underlying the Arabidopsis circadian clock. Plant Cell Physiol **52:** 1709–1718

Nieto C, López-Salmerón V, Davière JM, Prat S (2015) ELF3-PIF4 interaction regulates plant growth independently of the Evening Complex. Curr Biol **25:** 187–193

Niwa Y, Yamashino T, Mizuno T (2009) The circadian clock regulates the photoperiodic response of hypocotyl elongation through a coincidence mechanism in Arabidopsis thaliana. Plant Cell Physiol **50:** 838–854

Nozue K, Covington MF, Duek PD, Lorrain S, Fankhauser C, Harmer SL, Maloof JN (2007) Rhythmic growth explained by coincidence between internal and external cues. Nature **448:** 358–361

Nusinow DA, Helfer A, Hamilton EE, King JJ, Imaizumi T, Schultz TF, Farré EM, Kay SA (2011) The ELF4-ELF3-LUX complex links the circadian clock to diurnal control of hypocotyl growth. Nature **475:** 398–402

Pal SK, Liput M, Piques M, Ishihara H, Obata T, Martins MCM, Sulpice R, van Dongen JT, Fernie AR, Yadav UP, et al (2013) Diurnal changes of polysome loading track sucrose content in the rosette of wild-type Arabidopsis and the starchless *pgm* mutant. Plant Physiol **162:** 1246–1265

Pantin F, Fanciullino AL, Massonnet C, Dauzat M, Simonneau T, Muller B (2013) Buffering growth variations against water deficits through timely carbon usage. Front Plant Sci **4:** 483

Pantin F, Simonneau T, Muller B (2012) Coming of leaf age: control of growth by hydraulics and metabolics during leaf ontogeny. New Phytol **196:** 349–366

Pantin F, Simonneau T, Rolland G, Dauzat M, Muller B (2011) Control of leaf expansion: a developmental switch from metabolics to hydraulics. Plant Physiol **156:** 803–815

Paparelli E, Parlanti S, Gonzali S, Novi G, Mariotti L, Ceccarelli N, van Dongen JT, Kölling K, Zeeman SC, Perata P (2013) Nighttime sugar starvation orchestrates gibberellin biosynthesis and plant growth in *Arabidopsis*. Plant Cell **25:** 3760–3769

Perwass C, Wietzke L (2012) Single lens 3D-camera with extended depth-of-field. Proc SPIE **8291:** 829108–829115

Poiré R, Wiese-Klinkenberg A, Parent B, Mielewczik M, Schurr U, Tardieu F, Walter A (2010) Diel time-courses of leaf growth in monocot and dicot species: endogenous rhythms and temperature effects. J Exp Bot **61:** 1751–1759

Pokhilko A, Fernández AP, Edwards KD, Southern MM, Halliday KJ, Millar AJ (2012) The clock gene circuit in Arabidopsis includes a repressilator with additional feedback loops. Mol Syst Biol **8:** 574

Polko JK, van Zanten M, van Rooij JA, Marée AFM, Voesenek LACJ, Peeters AJM, Pierik R (2012) Ethylene-induced differential petiole growth in Arabidopsis thaliana involves local microtubule reorientation and cell expansion. New Phytol **193:** 339–348

Poorter H, Nagel O (2000) The role of biomass allocation in the growth response of plants to different levels of light, CO_2, nutrients and water: a quantitative review. Funct Plant Biol **27:** 1191

Poorter H, Walter A, Fiorani F, Schurr U, Niinemets Ü (2009) Metaphenomics: building a unified framework for interpreting plant growth responses to diverse environmental variables. Comp Biochem Physiol A Mol Integr Physiol **153:** S224

Pyl ET, Piques M, Ivakov A, Schulze W, Ishihara H, Stitt M, Sulpice R (2012) Metabolism and growth in *Arabidopsis* depend on the daytime temperature but are temperature-compensated against cool nights. Plant Cell **24:** 2443–2469

Rauf M, Arif M, Fisahn J, Xue GP, Balazadeh S, Mueller-Roeber B (2013) NAC transcription factor speedy hyponastic growth regulates flooding-induced leaf movement in *Arabidopsis*. Plant Cell **25:** 4941–4955

Rousseeuw PJ (1987) Silhouettes: a graphical aid to the interpretation and validation of cluster analysis. J Comput Appl Math **20:** 53–65

Ruts T, Matsubara S, Wiese-Klinkenberg A, Walter A (2012) Aberrant temporal growth pattern and morphology of root and shoot caused by a defective circadian clock in Arabidopsis thaliana. Plant J **72:** 154–161

Salah H, Tardieu F (1997) Control of leaf expansion rate of droughted maize plants under fluctuating evaporative demand (a superposition of hydraulic and chemical messages?). Plant Physiol **114:** 893–900

Salomé PA, McClung CR (2005) PSEUDO-RESPONSE REGULATOR 7 and 9 are partially redundant genes essential for the temperature responsiveness of the *Arabidopsis* circadian clock. Plant Cell **17:** 791–803

Scialdone A, Mugford ST, Feike D, Skeffington A, Borrill P, Graf A, Smith AM, Howard M (2013) Arabidopsis plants perform arithmetic division to prevent starvation at night. eLife **2:** e00669

Seaton DD, Smith RW, Song YH, MacGregor DR, Stewart K, Steel G, Foreman J, Penfield S, Imaizumi T, Millar AJ, et al (2015) Linked circadian outputs control elongation growth and flowering in response to photoperiod and temperature. Mol Syst Biol **11:** 776

Smith AM, Stitt M (2007) Coordination of carbon supply and plant growth. Plant Cell Environ **30:** 1126–1149

Smith HE (1982) Light quality, photoperception, and plant strategy. Annu Rev Plant Physiol **33:** 481–518

Song YH, Shim JS, Kinmonth-Schultz HA, Imaizumi T (2015) Photoperiodic flowering: time measurement mechanisms in leaves. Annu Rev Plant Biol **66:** 441–464

Spalding EP, Miller ND (2013) Image analysis is driving a renaissance in growth measurement. Curr Opin Plant Biol **16:** 100–104

Stitt M, Zeeman SC (2012) Starch turnover: pathways, regulation and role in growth. Curr Opin Plant Biol **15:** 282–292

Sulpice R, Flis A, Ivakov AA, Apelt F, Krohn N, Encke B, Abel C, Feil R, Lunn JE, Stitt M (2014) Arabidopsis coordinates the diurnal regulation of carbon allocation and growth across a wide range of photoperiods. Mol Plant **7:** 137–155

Sun J, Qi L, Li Y, Chu J, Li C (2012) PIF4-mediated activation of YUCCA8 expression integrates temperature into the auxin pathway in regulating Arabidopsis hypocotyl growth. PLoS Genet **8:** e1002594

Tang AC, Boyer JS (2008) Xylem tension affects growth-induced water potential and daily elongation of maize leaves. J Exp Bot **59:** 753–764

Tardieu F, Granier C, Muller B (1999) Modelling leaf expansion in a fluctuating environment: are changes in specific leaf area a consequence of changes in expansion rate? New Phytol **143:** 33–44

Usadel B, Bläsing OE, Gibon Y, Retzlaff K, Höhne M, Günther M, Stitt M (2008) Global transcript levels respond to small changes of the carbon status during progressive exhaustion of carbohydrates in Arabidopsis rosettes. Plant Physiol **146:** 1834–1861

Whippo CW, Hangarter RP (2009) The "sensational" power of movement in plants: a Darwinian system for studying the evolution of behavior. Am J Bot **96:** 2115–2127

Wiese A, Christ MM, Virnich O, Schurr U, Walter A (2007) Spatio-temporal leaf growth patterns of Arabidopsis thaliana and evidence for sugar control of the diel leaf growth cycle. New Phytol **174:** 752–761

Yanovsky MJ, Kay SA (2002) Molecular basis of seasonal time measurement in Arabidopsis. Nature **419:** 308–312

Yazdanbakhsh N, Sulpice R, Graf A, Stitt M, Fisahn J (2011) Circadian control of root elongation and C partitioning in Arabidopsis thaliana. Plant Cell Environ **34:** 877–894

Zagotta MT, Hicks KA, Jacobs CI, Young JC, Hangarter RP, Meeks-Wagner DR (1996) The Arabidopsis ELF3 gene regulates vegetative photomorphogenesis and the photoperiodic induction of flowering. Plant J **10:** 691–702